

Modelling of ocean waves with the Alber equation: application to non-parametric spectra and generalization to crossing seas

Agissilaos G. Athanassoulis¹ and Odin Gramstad²

¹Department of Mathematics, University of Dundee

²Hydrodynamics, MetOcean & SRA, Energy Systems, DNV

Wednesday 18th May, 2022

Abstract

We study the Alber equation, a phase-averaged second-moment model for the statistics of a wavefield, derived under a narrowbandedness assumption. More specifically, we use the Alber equation and its associated instability condition to quantify how close a given non-parametric spectrum is to being modulationally unstable, and apply this to a dataset of 100 non-parametric spectra provided by the Norwegian Meteorological Institute. The vast majority of realistic spectra turn out to be stable, but the “proximity to instability” metric is seen to correlate strongly with their steepness and Benjamin-Feir Index (BFI). Moreover, upon comparing with phase-resolved broadband Monte Carlo simulations, the kurtosis and probability of extreme waves for each sea state wavefield are also seen to correlate well with its “proximity to instability”. Finally, in order to extend this approach to crossing seas, we derive a generalized Alber equation starting from a system of nonlinear Schrödinger equations modelling crossing seas. We also derive the associated 2-dimensional instability condition.

Keywords: ocean waves, Alber equation, modulation instability, rogue waves, crossing seas

Contents

1	Introduction	2
2	Ocean wave modelling with the Alber equation	3
2.1	Derivation	3
2.2	The stability-of-homogeneity question	4
2.3	Implications	5
2.3.1	Quantifying stability	5
2.3.2	Shape of the spectrum	7
2.3.3	Emergence of coherent structures	9
3	Main results	9
3.1	The Alber equation for crossing seas	9
3.2	Unidirectional non-parametric spectra	10
3.2.1	The data	10
3.2.2	The algorithm for checking the instability condition	11
3.2.3	Summary & Comparison with phase-resolved Monte Carlo	12
4	Proof of Theorem 3.1	15

1 Introduction

Ocean waves are a very active field of mathematical modelling and analysis. The first principles hydrodynamic models for gravity waves are by now well understood [1, 31, 32]. An array of approximate models is well established and widely used, including the nonlinear Schrödinger equation (NLS) and its variants [10, 51], the Zakharov equation [53], the coupled-mode systems [9], the High Order Spectral Method (HOSM) [20, 52, 21] and others. (In shallow water an even larger collection of models is being used, but here we focus on deep water.) One reason for the wide use of approximate models in oceanography is the need to study large wavefields, with hundreds or thousands of individual wavelengths. Thus there is a trade-off between hydrodynamic fidelity and the ability to scale up models, as well as the accessibility of powerful qualitative insights.

In fact, actual ocean waves include multi-physics and non-differentiable phenomena, such as wind forcing, wave breaking etc. These are not accounted for in the classical “exact” hydrodynamic model anyway, and are still being understood on different levels [14, 13, 6, 15, 27].

In this paper we will use *stochastic modelling* of ocean waves and, furthermore, explore *what phase-averaged stochastic models may reveal about rogue waves in particular*. This will lead us to novel mathematical results; it is also worth mentioning that this kind of overall approach has been identified as a priority within the broader marine research & industry community [24].

The most well-known stochastic models for ocean waves include the CSY equation [18, 3, 4], Hasselmann’s equation [26] and the Alber equation [2] that we will focus on here. For a recent review of various stochastic models one can see [48]. Broadly speaking, they are **moment equations**, starting from **phase-resolved equations** for the sea surface (such as Zakharov’s equation or the NLS) as an approximation for deterministic wave dynamics. One then takes stochastic moments of the deterministic equations; due to the nonlinearity of these equations, an infinite hierarchy of moments is produced. A **gaussian second-order moment closure** is then used, to produce a closed equation for the second stochastic moment. The resulting equation is **phase-averaged**, meaning that it no longer resolves individual wave peaks and troughs, but instead the evolution and propagation of the statistics of the wavefield.

These are all **phase-averaged second-moment** schemes, and a key approximation step is the gaussian moment closure. This is of course not exact, but in many cases the free surface is indeed close to being gaussian [29, 37], making the gaussian closure plausible. It is important to keep in mind that fidelity to the deterministic, phase-resolved model is not the only consideration: for example, the exact infinite hierarchy of moments, is not just more complicated as a mathematical model: **it is impossible to initialize meaningfully**. The vast majority of synoptic data collected from the ocean is, or can be converted to, some kind of second moment [37]. There is some data involving moderately higher moments, but very little data or know-how exists for moments higher than 4th order.

The question of using realistic data for initialisation is extremely important; all the more so in the study of extreme sea states and rogue waves. For example, **every deterministic model can produce “rogue waves” on demand, by carefully preparing particular initial conditions**; however, the real-life question is **how often would these “initial conditions leading to rogue waves” realistically appear?** A stochastic approach can directly attack this question e.g. by a phase-resolved Monte Carlo approach [49]; this has a number of advantages, but is clearly expensive to be applied indiscriminantly. Another possibility would be using phase averaged stochastic models, like the moment equations discussed above, to directly investigate whether a sea state is likely to support the rapid concentrations of energy. That way sea states of interest could be selected and computational resources focused on them. In fact,

it appears that the sea states highlighted as more unstable by the Alber equation do turn out to exhibit a higher probability of extreme events in a phase-resolved Monte Carlo simulation (details in Section 3.2.3 and Figure 8).

2 Ocean wave modelling with the Alber equation

2.1 Derivation

The cubic focusing nonlinear Schrödinger equation (NLS)

$$i\partial_t u - p\Delta u - q|u|^2 u = 0. \quad (1)$$

is an approximate model for the **envelope** of a narrow-banded wavetrain with **carrier wavenumber** k_0 along its direction of propagation (unidirectional propagation), cf. e.g. [16]. Thus, in deep water the sea surface elevation is related to the complex-valued envelope $u(x, t)$ through

$$\eta(x, t) = \text{Re} \left[u(x, t) e^{i(k_0 x - \omega_0 t)} \right], \quad \omega_0 = \sqrt{gk_0}.$$

The coefficients of the equation also depend on k_0 ,

$$p = \frac{\sqrt{g}}{8k_0^{\frac{3}{2}}}, \quad q = \frac{\sqrt{g}}{2} k_0^{\frac{5}{2}}.$$

This is an asymptotic model, where the order parameter is the steepness of the waves, and moreover assumes narrow-bandedness of the wavefield around k_0 . The NLS and its variants are widely used as relevant to a wide array of realistic scenarios [49].¹ A different kind of limitation of the NLS is that it is a **deterministic phase-resolved model; i.e. any prediction with it will not be better or more accurate than the initial condition used.** But realistic wave-systems are not widely available as phase-resolved initial conditions, as opposed to power spectra. In that context, Alber [2] proposed generating a second-order moment equation from the NLS. Denoting by

$$R(x, y, t) = \mathbb{E}[u(x, t)\bar{u}(y, t)]$$

the autocorrelation of the envelope u , one obtains

$$i\partial_t R(x, y, t) + p(\Delta_x - \Delta_y) R(x, y, t) + q\mathbb{E}\left[u(x, t)\bar{u}(y, t)[u(x, t)\bar{u}(x, t) - u(y, t)\bar{u}(y, t)]\right] = 0. \quad (2)$$

By using the gaussian closure

$$\mathbb{E}[|u(\alpha, t)|^2 u(\alpha, t)\bar{u}(\beta, t)] = 2R(\alpha, \alpha, t)R(\alpha, \beta, t), \quad (3)$$

the autocorrelation can now be seen to satisfy

$$i\partial_t R(x, y, t) + p(\Delta_x - \Delta_y) R(x, y, t) + 2qR(x, y, t)[R(x, x, t) - R(y, y, t)] = 0. \quad (4)$$

A key restriction the Alber equation inherits from its starting point, the NLS equation, is **narrow-bandedness**. This is arguably not too restrictive for unidirectional sea states [49]; however it completely fails for crossing seas, i.e. sea states where several different directions carry substantial wave energy. To address this limitation, we will derive a generalized Alber equation valid in a crossing seas scenario. This is made possible by starting from a system of NLS equations describing the crossing wavetrains which was derived in [25]. The resulting generalized Alber equation is reported in Section 3, and derived in detail in Section 4. Crossing seas are receiving increased attention as a possible incubator of rogue waves [40, 23], so it is significant to have a moment equation applicable to such scenarios.

¹There are some key facts here; water waves cannot get too steep, since they break at a slope of about 0.13, and typically they are quite less steep than that. Moreover, wavelengths for gravity waves vary over no more than two orders of magnitudes ($\sim 5 - 500m$). In fact, sea-state spectra are known to often be more narrowly supported even within that range. In contrast, **crossing seas** (i.e. $O(1)$ wave-systems coming from different directions) cannot be considered narrowband due to the different directions; thus, they provide a prime example of a realistic situation where the NLS (1) would *not* be a satisfactory model.

2.2 The stability-of-homogeneity question

It is empirically known that sea-states are typically homogeneous and stationary, at least for appropriate lengthscales and timescales [29, 37, 30, 50]. This feature is reflected in the Alber equation; for example observe that $R(x, y, t) = \Gamma(x - y)$ is a solution of equation (4) for any smooth function Γ . The next step is to investigate the stability of such homogeneous and stationary solutions: let us consider a **weakly inhomogeneous initial sea-state**, i.e. assume that the autocorrelation is initially of the form

$$R(x, y, 0) = \mathbb{E}[u(x, 0)\bar{u}(y, 0)] = \Gamma(x - y) + \epsilon\rho(x, y, 0), \quad \epsilon \ll 1 \quad (5)$$

for some “nice” functions Γ, ρ . By inserting eq. (5) in eq. (4) one can reformulate the problem in terms of the inhomogeneity ρ ,

$$i\partial_t \rho(x, y, t) + p(\Delta_x - \Delta_y) R(x, y, t) + 2q[\Gamma(x - y) + \epsilon\rho(x, y, t)][\rho(x, x, t) - \rho(y, y, t)] = 0. \quad (6)$$

So stability for homogeneous state-states is controlled by the boundedness (or lack thereof) of the inhomogeneity ρ in equation (6). Can ρ grow in time to the extent that $\epsilon\rho(x, y, t)$ is no longer small? Or is there a guarantee that ρ stays bounded? In the latter case of stability, the autocorrelation will simply stay close to $\Gamma(x - y)$ for all times. In the unstable case however, even if initially very close to homogeneous, the autocorrelation could develop significant inhomogeneities.

In [2] a sufficient condition for linear instability was derived in terms of the **spectrum** $S(k)$ corresponding to the autocorrelation function $\Gamma(x - y)$, $S(k) = \mathcal{F}_{y \rightarrow k}[\Gamma(y)]$. Indeed, it was shown that the homogeneous sea-state with autocorrelation $\Gamma(x - y)$ is unstable if, for some $X \in \mathbb{R}$, there exists $\Omega(X) \in \mathbb{C}$ so that

$$1 + \omega_0 k_0^2 \int_k \frac{S(k + \frac{X}{2}) - S(k - \frac{X}{2})}{\Omega + \frac{\omega_0}{4k_0^2} kX} dk = 0. \quad (7)$$

This was called an “eigenvalue relation” in [2]; we will call it an “instability condition”. In [7] it was further shown that if the instability condition does not hold then linear stability follows. The instability condition (7) itself can be refined in two ways: one concerns a technical issue related to $X = 0$. However, the more serious one is that in (7) we are asked to guarantee the existence or not of solutions for a non-linear system of two equations (the real and imaginary part of eq. (7)) in three real unknowns (X , $\text{Re } \Omega$, $\text{Im } \Omega$). This is not straightforward in general, and historically it has been a challenge in using the Alber equation more widely [22]. In [7] this condition is reformulated so that a more constructive way to check it can be found: by dividing both sides of the fraction by X and setting

$$X' = \frac{X}{k_0}, \quad \Omega' = -\frac{\Omega 4k_0}{X\omega_0}, \quad k' = \frac{k}{k_0},$$

eq. (7) becomes

$$\frac{1}{4\pi} = \frac{1}{\pi} k_0^3 \int_{k'} \frac{S((k' + \frac{X'}{2})k_0) - S((k' - \frac{X'}{2})k_0)}{\Omega' - k'} dk'$$

This becomes very simple if we recognize it as **the Hilbert transform of the divided difference of the rescaled spectrum**. So, denoting

$$P(k) := k_0^3 S(kk_0), \quad D_X P(k) = \begin{cases} \frac{P(k + \frac{X}{2}) - P(k - \frac{X}{2})}{X}, & X \neq 0 \\ P'(k), & X = 0. \end{cases}, \quad \mathbb{H}[u](x) = \frac{1}{\pi} \text{p.v.} \int_{t \in \mathbb{R}} \frac{u(t)}{x - t} dt \quad (8)$$

and dropping the primes, the condition for instability finally becomes

$$\exists X \in \mathbb{R} : \quad \exists \Omega = \Omega(X) \in \mathbb{C} : \quad \mathbb{H}[D_X P](\Omega) = \frac{1}{4\pi}. \quad (9)$$

The benefit is that now the argument principle² can be used to reformulate this to a constructive condition that we can directly check [43, 8, 7]. To that end we will also need to introduce the **signal transform**,

$$\mathbb{S}[u](x) := \mathbb{H}[u](x) - iu(x); \quad (10)$$

we are now ready to state the equivalent instability condition:

Definition 2.1 (Penrose-Alber condition). *Consider a homogeneous sea state with autocorrelation function $\Gamma(x - y)$ and carrier wavenumber k_0 , and denote $S(k) = \mathcal{F}_{y \rightarrow k}[\Gamma(y)]$, $P(k) := k_0^3 S(kk_0)$. Then, the sea state is Penrose-Alber unstable if*

$$d(\bar{\Gamma}, \frac{1}{4\pi}) = 0,$$

where

$$\Gamma_X := \{\mathbb{S}[D_X P(\cdot)](t), t \in \mathbb{R}\} \cup \{0\}, \quad \overset{\circ}{\Gamma}_X = \{z \in \mathbb{C} | z \text{ enclosed by } \Gamma_X\}, \quad \bar{\Gamma} := \overline{\bigcup_{X \in \mathbb{R}} \overset{\circ}{\Gamma}_X}. \quad (11)$$

Any X for which $1/4\pi \in \bar{\Gamma}_X$ is called an unstable wavenumber.

This notion of instability is equivalent to condition (9) [7].

We call this the Penrose-Alber instability condition after Alber’s “eigenvalue relation” (7) [2] and Penrose’s introduction of the argument principle in an analogous problem in plasma [43]. The point is that this formulation of the condition boils down to drawing closed curves on the complex plane, and looking whether the point $1/4\pi$ is inside or outside of them, cf. Figure 2. It was used in [7] to study parametric JONSWAP spectra; here we will apply it to non-parametric spectra as well.

This stability-of-homogeneity question that was first studied in [2] is in fact a variant of a much better known stability question. The **modulation instability (MI)** is well understood and widely studied in a phase-resolved setting, for a plane wave background [54]. It can easily be seen that a sequence of spectra approaching a plane wave $S(k) = a\delta(k - k_0)$ would become unstable in the Penrose-Alber sense. In fact, the Penrose-Alber instability is just the modulation instability for more general backgrounds than plane waves. A modulationally unstable sea state supports the rapid concentrations of energy – a possible mechanism for the formation of rogue waves [42, 39, 41, 8].

Unlike the classical MI, where every plane-wave solution is always unstable, a spectrum can be stable or unstable in the Penrose-Alber sense. In the case of stability, the homogeneity of the sea-state is robust, and small perturbations will merely disperse. **In these cases, despite having a focusing nonlinearity and infinite energy present, the dynamics are going to be dominated by the linear dispersion for all times.** This is a familiar leading order approximation in ocean waves, but it doesn’t necessarily have a name to itself in an oceanographic context. As the rigorous stability analysis of [7] highlighted, mathematically this stable regime looks exactly like what is called **Landau damping** for Vlasov equations (indeed this parallel was also drawn before [38]).

2.3 Implications

2.3.1 Quantifying stability

As was seen just above, a key feature of the Alber equation is a classification of a given spectrum as either stable or unstable. A careful look at the asymptotics can offer more nuance. For example, consider two sea states: one with a barely stable spectrum $S(k)$, and the other with a slightly perturbed version, e.g. $(1 + \varepsilon)S(k)$, so that it becomes barely unstable. These sea states will behave similarly on physically

²For a holomorphic function f defined on a closed domain $A \subseteq \mathbb{C}$, $f : A \rightarrow \mathbb{C}$, it follows that $z \in f(A)$ if and only if the curve $f(\partial A)$ is circumscribed around $z \in \mathbb{C}$.

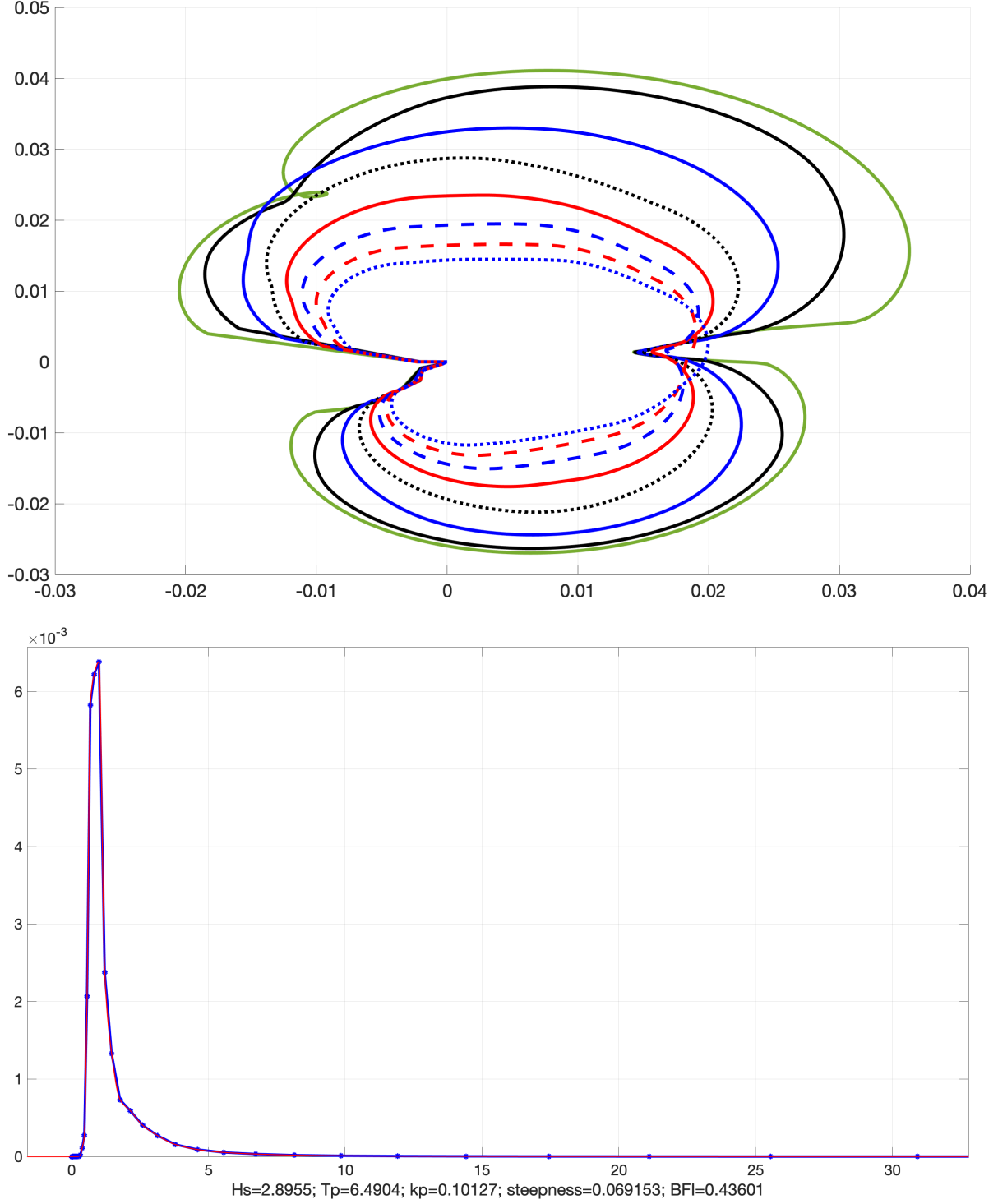


Figure 1: **Top:** Curves Γ_X for nonparametric spectrum no. 11300 on the complex plane. In each graph, the smaller closed curves correspond to larger $|X|$; here $X = (1 + 120 \cdot n)5 \cdot 10^{-4}$, $n = 0, \dots, 7$. Taking $0 < X < 5 \cdot 10^{-4}$ does not change the outermost curves noticeably, as $D_X P$ has effectively converged to P' . The real number $1/4\pi \approx 0.08$ is *not* circumscribed by any of the curves, i.e. the spectrum does *not* exhibit modulation instability. On the other hand, spectrum no. 11300 comes as close to being unstable as any spectrum in this dataset. See also Figure 2. **Bottom:** The rescaled spectrum no. 11300. If $S(k)$ is the raw spectrum, then the rescaled one is $P(k) := k_p^3 S(kk_p)$, cf. (8). Here the “carrier wavenumber” k_0 is taken to be the **peak wavenumber** k_p , $S(k_p) = \max_k S(k)$. It is a clearly unimodal spectrum, with a high steepness of almost 7%.

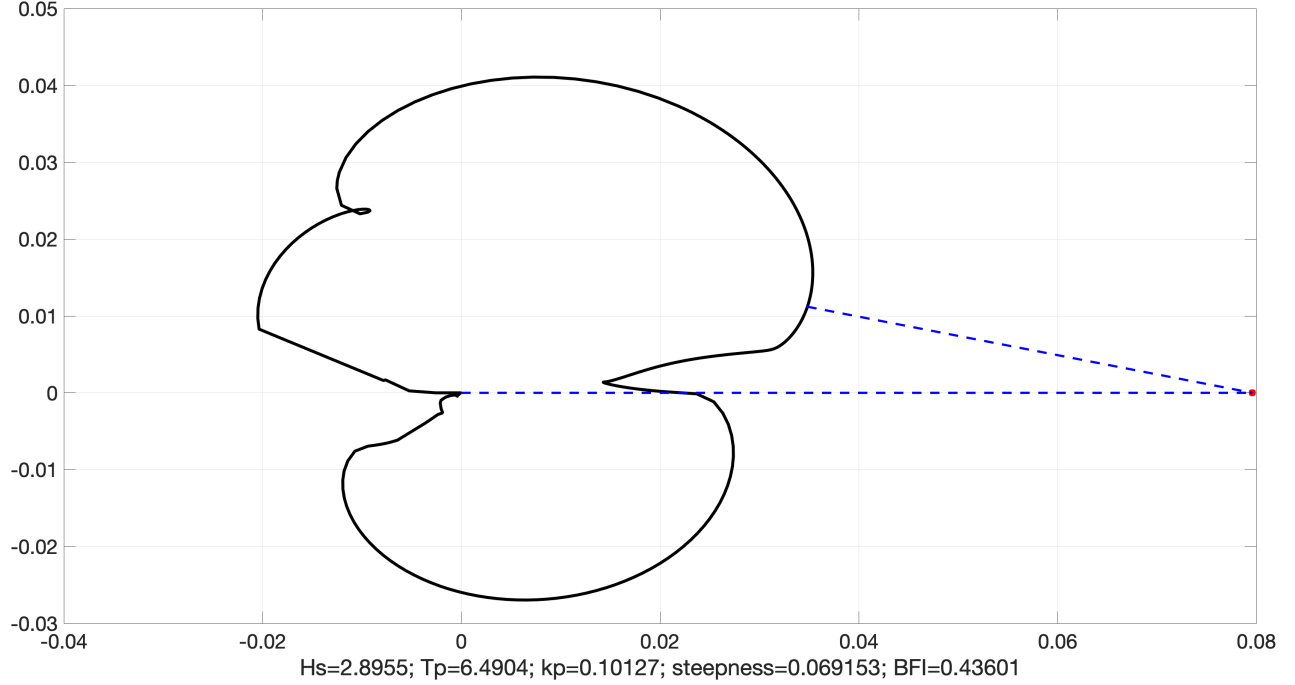


Figure 2: We can quantify how close each spectrum is to being modulationally unstable by measuring the distance by between Γ_X and $1/4\pi$ (plotted here as a red star). In practice, it suffices to do this for $X \approx 5 \cdot 10^{-4}$, as much smaller values of X yield similar results, and large values of X lead to smaller and smaller curves, cf. Figure 1. So now we can say that spectrum no. 11300 has come something like 42% of how far out it would need to be in order to be modulationally unstable. See Figure 7 for a more systematic application of this idea to our dataset.

realistic timescales – as one would intuitively expect. In particular, there is not a violent bifurcation from Landau damping to modulation instability, but rather a gradual transition [7, 8]. On the other hand, as we will see in some detail here, a spectrum exhibiting Landau damping can be “more stable” than another spectrum which also exhibits Landau damping. In short, the *effective stability* of a spectrum is better thought of as belonging to a continuous range of values rather than a binary “stable / unstable” classification. One of the results of this paper is a non-dimensional index quantifying this “effective stability”, cf. Figures 2, 7.

This is important because, even in the presence of Landau damping (i.e. for “stable” spectra) *only small enough inhomogeneities are guaranteed to disperse*. Large inhomogeneities are not well understood, and could very well behave differently. This is a harder mathematical problem, because now we are talking about large perturbations and by definition asymptotics are not as powerful. To better understand this question there is a numerical requirement (efficient and reliable solvers for the Alber equation both in the stable and unstable regime) as well as a data requirement (quantify how large inhomogeneities are in the ocean; this may be possible e.g. with X-band radar imaging [12]). It is quite possible that, if a spectrum is close enough to MI the likelihood of nonlinear events under realistic perturbations may substantially increase, even if technically the spectrum does exhibit Landau damping.

2.3.2 Shape of the spectrum

The fundamental scaling of the problem shows that the vast majority of plausible sea states would be stable, in accordance with the well-known fact that linearized dynamics very often do a good job in de-

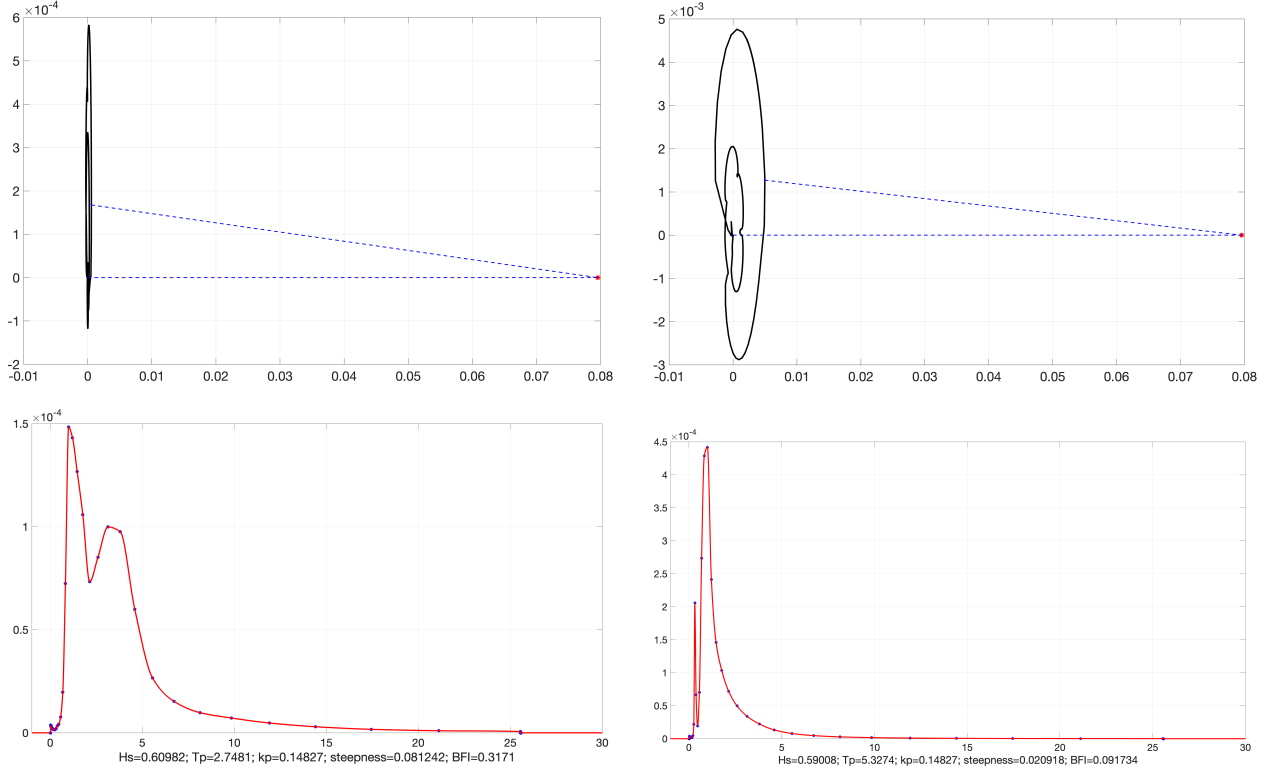


Figure 3: **Top left:** complex plane plot of Γ_X for spectrum no. 5498. **Top right:** complex plane plot of Γ_X for spectrum no. 13616. **Bottom left:** Rescaled spectrum no. 5498. (Rescaling is as in eq. (8). Blue points are data points, red line is the smooth interpolation used.) **Bottom right:** Rescaled spectrum no. 13616. These are both bimodal spectra, with the same peak wavenumber and very similar H_s . Here the shape comes into play in a big way. While both spectra are rather stable, the spectrum with the substantially larger steepness ends up noticeably further away from modulation instability compared to the spectrum with the smaller steepness. This is a case that highlights the issue of selecting the “carrier wavenumber”, as other choices than the peak wavenumber would also be reasonable (e.g. median wavenumber) and could lead to noticeable differences. A broadband moment equation such as the CSY equation would overcome this issue, as there would be no need to choose a carrier wavenumber at all.

scribing phase-averaged energy propagation. On the other hand, it seems that instability is potentially within reach, i.e. the scaling of the problem does not make instability so far removed as to be considered impossible. This much was established in [7, 22, 46], working in the context of fitted parametric JONSWAP spectra. While fitted spectra are widely used, the question remains whether the exact shape of the spectrum can make a substantial difference. In this paper we work with a set of nonparametric unidirectional spectra. **A key objective is to see just how much the details of the spectral shape matter with regard to the Penrose-Alber instability condition.** A striking example of the role of the shape can be found in Figure 3. For spectra that are not strongly unimodal, the question of choosing the carrier wavenumber also emerges as significant.

The methodology and the results of our investigation are described in detail in Section 3.2. In a nutshell, we don’t find any unstable spectra among the sea states we examine; we do find some that are substantially closer to being unstable than others, even if they have comparable H_s, k_p . The idea of Figure 2 can be expanded to a non-dimensional measure of how close a spectrum is to being unstable. This is found to correlate well with BFI and steepness for strongly unimodal spectra; see also Figure 7. It is also found to correlate well with commonly used metrics for prevalence of extreme waves in a phase-resolved

Monte Carlo simulation, see also Figure 8.

2.3.3 Emergence of coherent structures

Another area with many open questions is what happens when instability arises. For modulationally unstable spectra with a small perturbation, formal asymptotics can be used to describe the early evolution of the instability. A particular coherent structure emerges, determined by the unstable wavenumbers for the particular spectrum, and their rate of growth, rather than the initial small perturbation. In that sense the coherent structure, at least in its early stages, is determined by the spectrum and the Penrose-Alber instability analysis suffices to predict it [8]. Rather surprisingly, the same kind of universal coherent structure was reported in a fully numerical study by van den Eijden et al. [19], for the *fully nonlinear stage of the instability*, cf. Figure 4. This is a direction where more work is needed, analytical, numerical and experimental.

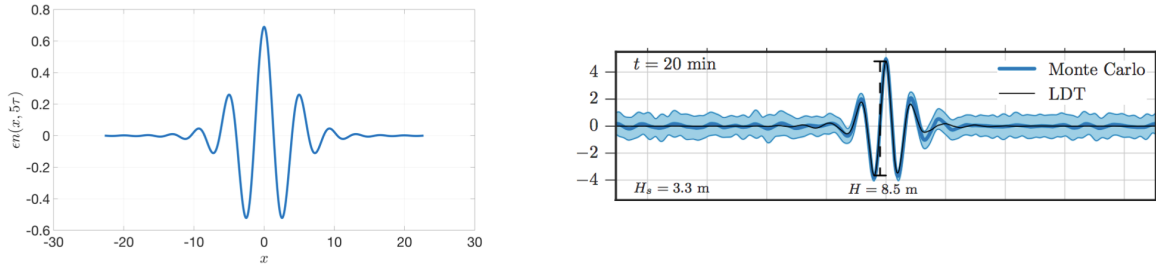


Figure 4: Predicted profile of emergent localized extreme events for NLS, according to [8] (**left**), and fully developed universal profile of rogue waves from [19] (**right**). (With permission from the authors.) This brings to mind the “three sisters” discussion [11, 33, 35, 36, 17, 5], or the Greek $\tau\rho\kappa\nu\mu\alpha$.

3 Main results

3.1 The Alber equation for crossing seas

Crossing seas constitute a genuinely two-dimensional scenario where modulation instability and rogue waves may be more prominent, but which is not still fully understood [23, 47, 25, 39, 40].

One way to study crossing seas is by deriving a coupled system of equations, each governing the evolution of one (quasi-uni-directional) wavefield. Let us denote the direction of propagation for the wavetrain A by $\mathbf{k}^A = (k_1^A, k_2^A)$ and for the wavetrain B by $\mathbf{k}^B = (k_1^B, k_2^B)$. The corresponding frequencies are

$$\omega^A = \sqrt{g|\mathbf{k}^A|}, \quad \omega^B = \sqrt{g|\mathbf{k}^B|} \quad (12)$$

for ocean waves (i.e. in the limit of infinite depth). In [25] the following system of NLS equations for the envelopes of two wavetrains, v^A, v^B , in two spatial dimensions is derived:

$$i \frac{d}{dt} v^A + i \mathbf{C}^A \cdot \nabla_x v^A + \alpha_1 \partial_{x_1}^2 v^A + \beta_1 \partial_{x_2}^2 v^A + \gamma_1 \partial_{x_1} \partial_{x_2} v^A + (\xi_1 |v^A|^2 + \zeta_1 |v^B|^2) v^A = 0, \quad (13)$$

$$i \frac{d}{dt} v^B + i \mathbf{C}^B \cdot \nabla_x v^B + \alpha_2 \partial_{x_1}^2 v^B + \beta_2 \partial_{x_2}^2 v^B + \gamma_2 \partial_{x_1} \partial_{x_2} v^B + (\xi_2 |v^B|^2 + \zeta_2 |v^A|^2) v^B = 0. \quad (14)$$

All the coefficients are completely determined in terms of $\mathbf{k}^A, \mathbf{k}^B$ [25].

Theorem 3.1. Consider the two crossing wavefields of equations (13), (14), and assume moreover that their autocorrelations at $t = 0$ can be written as

$$\mathbb{E}[v_A(\mathbf{x}, t)\overline{v_A(\mathbf{y}, t)}] = G^A(\mathbf{x} - \mathbf{y}) + \epsilon r_0(\mathbf{x}, \mathbf{y}), \quad \mathbb{E}[v_B(\mathbf{x}, t)\overline{v_B(\mathbf{y}, t)}] = G^B(\mathbf{x} - \mathbf{y}) + \epsilon s_0(\mathbf{x}, \mathbf{y}) \quad (15)$$

for some $\epsilon = o(1)$. Then the system (13), (14) exhibits **modulation instability** if

$$\exists \mathbf{P} \in \mathbb{R}^2, \omega \in \mathbb{C} : (1 - \xi_1 h^A(\mathbf{P}, \omega))(1 - \xi_2 h^B(\mathbf{P}, \omega)) = \zeta_1 \zeta_2 h^A(\mathbf{P}, \omega) h^B(\mathbf{P}, \omega) \quad (16)$$

where $h^A, h^B, \tilde{n}_A^0, \tilde{n}_B^0$ are defined in terms of the data of the problem in eq. (46)³. In that case, inhomogeneities are expected to grow in time.

On the other hand, if

$$\inf_{\substack{\operatorname{Re} \omega > 0 \\ \mathbf{P} \in \mathbb{R}^2}} \left| (1 - \xi_1 h^A(\mathbf{P}, \omega))(1 - \xi_2 h^B(\mathbf{P}, \omega)) - \zeta_1 \zeta_2 h^A(\mathbf{P}, \omega) h^B(\mathbf{P}, \omega) \right| = \kappa > 0 \quad (17)$$

and

$$\sup_{\substack{\operatorname{Re} \omega > 0 \\ \mathbf{P} \in \mathbb{R}^2}} (|h^A(\mathbf{P}, \omega)| + |h^B(\mathbf{P}, \omega)|) < +\infty \quad (18)$$

hold, then formally the problem exhibits **linear Landau damping**, i.e. inhomogeneities are expected to disperse and thus deviation from homogeneity to not grow noticeably.

The proof is found in Section 4.

Remark 3.2. Condition (17) is a Penrose-Alber condition for a system, and it is consistent with the condition for the scalar case. To see this assume that $v_B \rightarrow 0$; then, according to the definition of h^B (cf. eq. (46)) $h^B \rightarrow 0$ as well, and the condition becomes

$$\inf_{\substack{\operatorname{Re} \omega > 0 \\ \mathbf{P} \in \mathbb{R}^2}} \left| 1 - \xi_1 h^A(\mathbf{P}, \omega) \right| = \kappa > 0$$

which is exactly of the same type as requiring

$$\inf_{\substack{\operatorname{Re} \Omega > 0 \\ X \in \mathbb{R}}} \left| 1 - 4\pi \mathbb{H}[D_X P](\Omega) \right| = \kappa > 0$$

in the scalar case.

Just like in the scalar case, Condition (17) can also be resolved with the argument principle since, for each $\mathbf{P} \in \mathbb{R}^2$, it asks whether a holomorphic function attains the value 0 on the right half-plane, $\inf_{\operatorname{Re} \omega > 0, \mathbf{P} \in \mathbb{R}^2} |F_{\mathbf{P}}(\omega)| > \kappa$. Condition (18) apparently boils down to general regularity conditions for the spectra $\widehat{\Gamma}^A, \widehat{\Gamma}^B$. Working these ideas out in full detail will require the extension of some technical results to a non-standard “two-dimensional Hilbert transform” which arises here.

3.2 Unidirectional non-parametric spectra

3.2.1 The data

For the present analysis we have used 100 realistic nonparametric spectra taken from the Norwegian Meteorological Institute’s operational spectral wave model [45], which is a third-generation wave model based on WAM. The model provides wave spectra every hour for many locations in the North Atlantic. For

³Roughly speaking, h^A and h^B are transfer functions generated by the homogeneous backgrounds Γ^A, Γ^B , and $\tilde{n}_A^0, \tilde{n}_B^0$ express the free space (i.e. $\xi_1 = \xi_2 = \zeta_1 = \zeta_2 = 0$) evolution of the initial inhomogeneities.

this study 100 spectra from one specific location south-west of the Norwegian coast ($56^{\circ}36'N$, $3^{\circ}12'E$) were used. The selected spectra consisted of 80 spectra randomly selected from the full database (26 255 spectra covering the period from October 2016 to September 2019), as well as the 10 spectra having the largest mean wave steepness $\epsilon = H_s k_p / 2$ and the 10 spectra with the largest BFI-values, where BFI was defined from the frequency spectrum $E(\omega)$ as

$$\text{BFI} = \frac{\epsilon}{\sqrt{2}\delta_{\omega}},$$

where δ_{ω} is a measure for the frequency-bandwidth here defined in terms of Godas' peakedness factor Q_p , as suggested e.g. in [28]:

$$\delta_{\omega} = \frac{1}{Q_p \sqrt{\pi}} \quad \text{where} \quad Q_p = \frac{2}{m_0^2} \int \omega E^2(\omega) d\omega,$$

and where $m_0 = \int E(\omega) d\omega$ is the total energy of the spectrum.

Note that for the following analysis the original frequency spectra $E(\omega)$ were converted into wavenumber spectra $S(k)$ using the linear dispersion relation $\omega = \sqrt{gk}$.

3.2.2 The algorithm for checking the instability condition

Here we will implement the stability criterion of Definition 2.1 to a number of non-parametric ocean spectra. First of all we will rescale them $S(k) \mapsto P(k) := k_0^3 S(k \cdot k_0)$, where $k_0 = k_p$ is just the peak wavenumber. (Other ways of determining k_0 would give similar values; the end result would not differ by orders of magnitude, but it may not be negligible either in some cases.) The other operation we will need to do is interpolate the discrete data; this will be crucial in using high order quadrature methods, and also being able to evaluate $P(k)$ outside the provided range of wavenumbers (i.e. our piecewise polynomial must be identically zero outside that range). Splines are well suited to this task; the additional requirement is to minimize overshooting at maxima, as this could make a big difference with regard to our investigation. To that end we use the `pchip`, a piecewise polynomial interpolation routine in MATLAB that minimizes overshoot, cf. Figure 5.

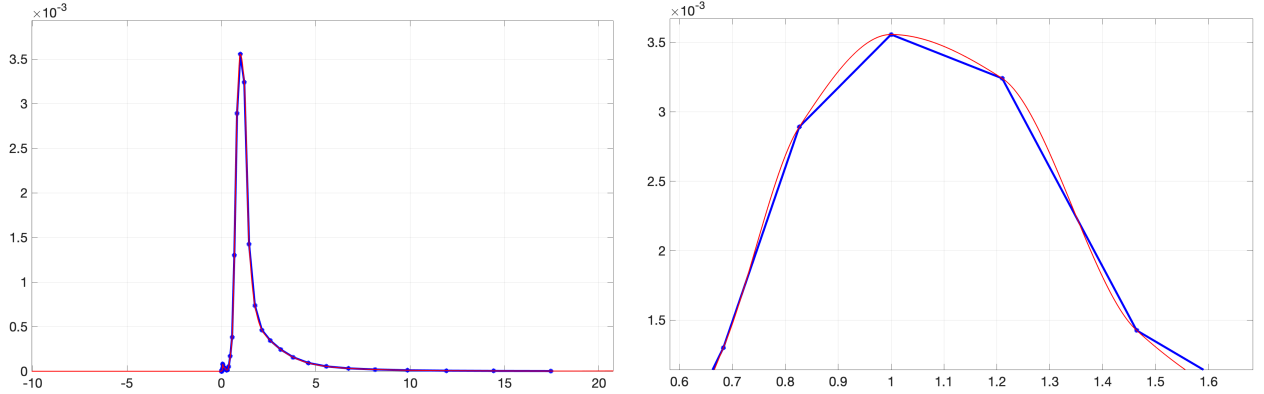


Figure 5: Blue points: data points. Blue line: linear interpolation of data. Red line: piecewise polynomial interpolation / extrapolation. This is the rescaled spectrum, therefore the maximum is always at $\xi = 1$.

The non-trivial part of the computation is the Hilbert transform, which is a singular integral. To that end we will use the Sokhotski-Plemelj formula,

$$\forall u \in C(\mathbb{R}) \cap L^1(\mathbb{R}) \quad \lim_{\eta \rightarrow 0^+} \frac{1}{\pi} \int \frac{u(s)}{t - s - (\sqrt{-1})\eta} ds = \mathbb{H}[u](t) - iu(t) = \mathbb{S}[u](t)$$

and truncate the limit by taking an appropriate $\eta = \text{compl_tol} \ll 1$. After extensive testing it is found that the result doesn't change noticeably once $\eta \approx 10^{-4}$. That way we avoid the singular integral. A detailed pseudocode for how the curve Γ_X is generated is presented in Algorithm 1.

It is a moderately heavy computation if a good approximation for all of Γ_X is required, as a few million points are typically required in order to achieve stringent error tolerances ($\sim 10^{-2}$ relative error tolerance or $\sim 10^{-6}$ absolute error tolerance). However, one can check stability more quickly, by checking only the points t_* where $D_X P(t_*) = 0$; these are the points where the curve Γ_X crosses the real axis. If it never crosses the real axis to the right of $1/4\pi$, then topologically $1/4\pi$ cannot possibly be in the interior of the curve.

Some more details involve the selection of X ; it is found that $X \ll 1$ will produce the curves that have the most chance of coming closer to $1/4\pi$, as when X increases the curves Γ_X shrink to zero, see Figure 1. Numerical testing shows that $X \approx 10^{-4}$ gives a good picture of what happens as $X \rightarrow 0$. So, if for $X \approx 10^{-4}$ Γ_X is not winding around $1/4\pi$, nor coming very close to it, we can accept the spectrum as stable. Finally, the grid t_i where $\mathbb{S}[D_X P](t_i)$ is evaluated has some interest; the effective support of $D_X P$ should be well resolved, and the most interesting areas are around the roots of $D_X P$ (which for small X are close to local extrema). Once $D_X P$ starts to decay strongly, there is no point in dedicating too many resources. A non-uniform grid can save substantial time, cf. Figure 6.

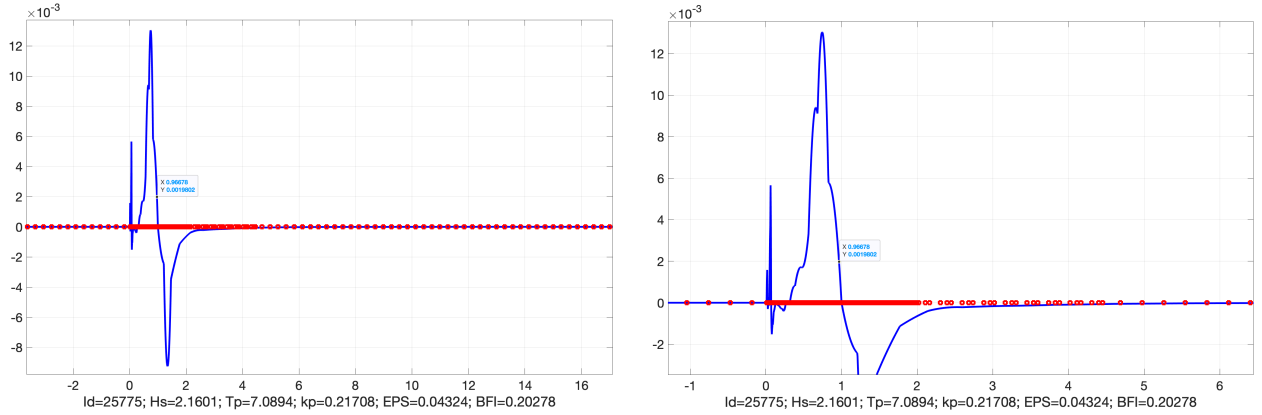


Figure 6: Plotting the divided difference $D_X P$ can help choose the points t_i where $\mathbb{S}[D_X P](t_i)$ is to be evaluated. Blue line: $D_X P(t)$. Red points: t_i chosen.

3.2.3 Summary & Comparison with phase-resolved Monte Carlo

All the non-parametric spectra examined were found to exhibit Landau damping, although a wide range of behaviours were found, spanning the range from near zero to nearly halfway through to MI; see Figures 3, 7. The shape of the spectrum was found to play a big role in cases departing from a strongly concentrated, unimodal profile, cf. Figure 3. The rescaled maximum of the spectrum $(k_p)^3 \cdot \max S(k)$ is found to correlate strongly with how close a spectrum is to MI, see Figure 7. Given that k_0^3 appears in the rescaling, it is clear that when there is ambiguity in choosing k_0 this will be enlarged with respect to the exact distance of Γ_X from $1/4\pi$, i.e. the computed distance from instability.

Moreover, for each of the 100 spectra selected for this study, we have run numerical simulations with the Higher Order Spectral Method (HOSM) [20, 52] in a Monte-Carlo approach where each spectrum were simulated 100 times with different initial random phases and random amplitudes each run. That is,

Algorithm 1 Pseudo-code for the computation of Γ_X

Input S_j, k_j (*Sampled values of wavenumber-resolved spectrum, $k_j \in [0.00479, 3.78]$.*)

Rescale $(S_j, k_j) \mapsto (k_0^3 S_j, k_j/k_0) = (P_j, \xi_j)$ (k_0 is simply taken to be the peak wavenumber.)

Interpolate $P(\xi)$

Set $\text{compl_tol} \sim 10^{-4}$, $\text{rel_tol} \sim 10^{-2}$, $\text{abs_tol} \sim 10^{-6}$

For $t_i := t_{\min}$ **to** t_{\max} **step** δt

While $\text{rel_err} > \text{rel_tol}$ **AND** $\text{abs_err} > \text{abs_tol}$

Integrate

$$I = \frac{1}{\pi} \int_s \frac{\frac{P(s+\frac{X}{2}) - P(s-\frac{X}{2})}{X}}{t_i - s - (\sqrt{-1}) \text{compl_tol}} ds$$

 using composite Simpson on two quadrature grids: a finer one and a coarser one, generating two approximations, **I_fine** and **I_coarse**. (*Fine grid has $3 \times$ the number of points compared to coarse grid.*)

Set $\text{rel_err} = \frac{|\text{I_fine} - \text{I_coarse}|}{\text{I_fine}}$, $\text{abs_err} = |\text{I_fine} - \text{I_coarse}|$.

End While

Set $\Gamma(t_i) = \text{I_fine}$

End For

Plot the line $\left(\text{Re } \Gamma_X(t_i), \text{Im } \Gamma_X(t_i) \right)$, $i = 1, 2, \dots$ and the point $(\frac{1}{4\pi}, 0)$

Check whether $(\frac{1}{4\pi}, 0)$ is inside Γ_X (*This can be done with the MATLAB `inpolygon` function.*)

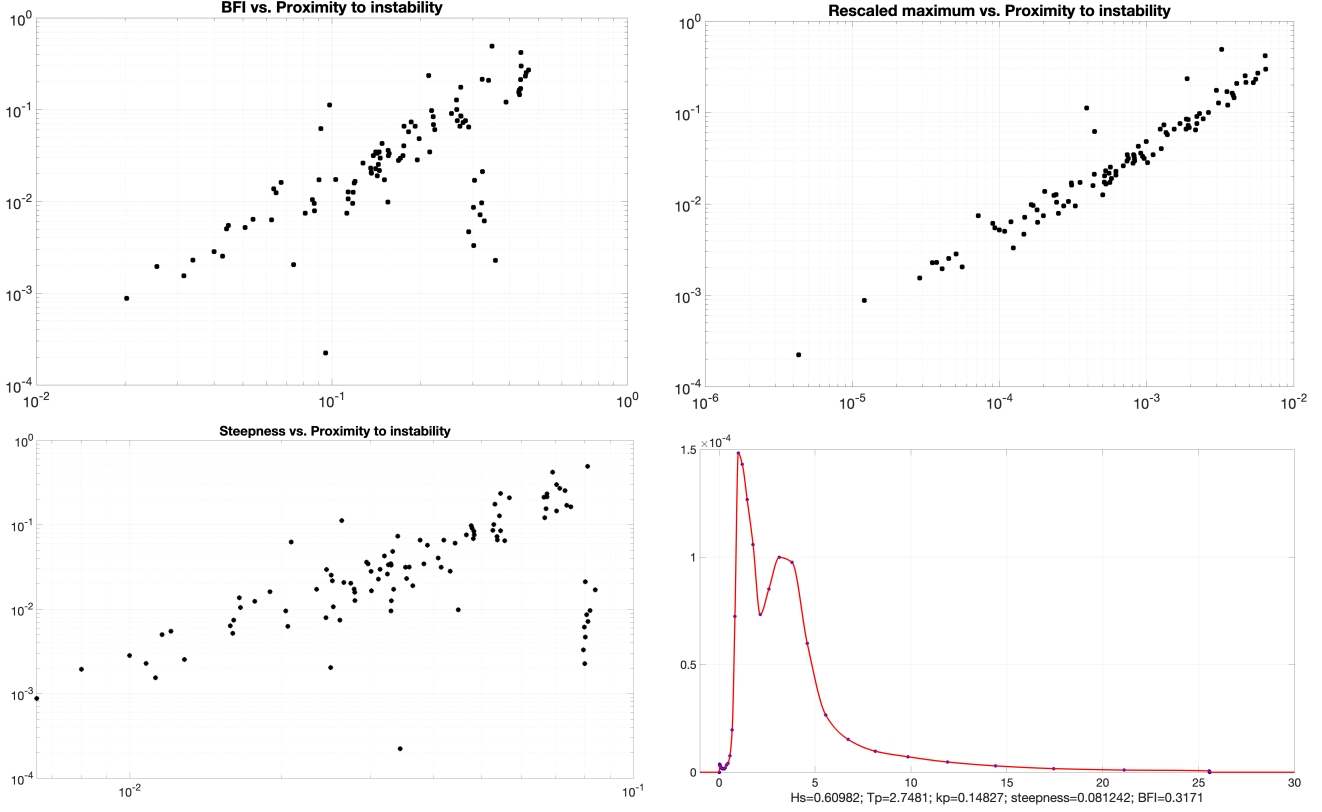


Figure 7: The new measure of distance between Γ_X and $1/4\pi$ shown in Figure 2 offers a quantitative, nondimensional way to assess how far a spectrum is from being modulationally unstable. The Benjamin-Feir Index (BFI) was introduced with a similar task in mind; so it is only natural to ask how well the two are correlated. To be precise we define as “proximity to instability” the quantity $1 - 4\pi \cdot d(\Gamma, 1/4\pi)$. This is 0 for the zero spectrum (“most stable”) and 1 for a modulationally unstable spectrum. In the **top left** graph above we see a log-log scatterplot of BFI v. proximity to instability. In the **top right** graph we see a similar scatterplot of the maximum of the rescaled spectrum ($\max P(k) = (k_p)^3 \max S(k)$) v. proximity to instability. In the **bottom left** graph we see a similar scatterplot with steepness v. proximity to instability. Most of the outliers in the BFI and steepness plots are bimodal spectra, such as the (rescaled) one seen in the **bottom right** graph. Overall BFI and steepness do a very good job of predicting proximity to instability for “sufficiently unimodal” spectra.

for a given spectrum $S(k)$ the initial surface elevation is in the form

$$\eta(x, t = 0) = \text{Re} \sum_{j=1}^n A_j \exp(ik_j x) \quad \text{where} \quad A_j = Z_j \sqrt{2S(k_j)\Delta k_j} \quad (19)$$

where $\Delta k_j = k_{j+1} - k_j$ is the grid spacing between the discrete wavenumbers and where Z_j are independent complex standard normal variables. That is, the real and imaginary parts of Z_j are independent normally distributed random variables with zero mean and variance $1/2$, meaning that $|Z_j|$ are Rayleigh distributed with parameter $\sigma = 1/\sqrt{2}$ so that $E[|Z_j|^2] = 1$ and $E[|A_j|^2] = 2S(k_j)\Delta k_j$, and the phases $\text{Arg}(Z_j)$ are uniformly distributed on $[0, 2\pi)$.

HOSM applies a regular discretization of the wavenumbers so that $\Delta k = 2\pi/x_{max} = 2\pi/n\Delta x$, leading to a periodic domain of length x_{max} in space. In the present simulations we have used $n = 1024$, representing wavenumbers up to $k_{max} = 8k_p$, where k_p is the spectral peak. This means that $\Delta k = 2k_{max}/n$, corresponding to $\Delta x = \lambda_p/16$ and $x_{max} = 64\lambda_p$, where $\lambda_p = 2\pi/k_p$ is the wavelength of the peak wavenumber.

Each simulation was run for 30 minutes, from which time series of surface elevation were extracted from four locations distributed over the simulation domain. Thus, 200 hours of surface elevation time series were obtained for each sea state. Since here we are interested in relations between the instability (or proximity of such) obtained from the stochastic approach (i.e. Alber equation) and the occurrence of rogue and extreme events in random realizations of the sea states (i.e. phase-resolved Monte-Carlo simulations), we will consider the following parameters related to the occurrence of extreme wave events: **the sea surface kurtosis and the probability of extreme wave crests.**

The sea surface kurtosis is a measure for how much the tail of the distribution deviates from Gaussian statistics. For a Gaussian distribution the kurtosis is equal to zero, while a positive value for kurtosis means indicates more large events than in a Gaussian population. Hence, the kurtosis is often used as an indicator for the probability of extreme and rogue waves. Secondly we consider **the probability that a wave crest, defined as the maximum between each zero-crossing of the surface elevation, exceeds 1.25 times the significant wave height H_s ; $P(C > 1.25H_s)$.** This is a common definition of a rogue wave, which under linear assumption (Rayleigh distributed crests) has the probability $P(C > 1.25H_s) = \exp(-12.5)$.

Figure 8 shows the kurtosis and “rogue wave probability” for each spectrum calculated from the HOSM simulations, plotted against the proximity to instability, $1 - 4\pi d(\Gamma, 1/4\pi)$. It is interesting to note that pronounced outliers in these plots all correspond to bimodal spectra with the maximum being the first peak (smaller k ; like spectrum no. 5498 in Figure 3). Thus their proximity to instability is somewhat underestimated, compared e.g. with unimodal spectra, or bimodal spectra where the second peak is larger (as in spectrum no. 13616 in Figure 3). This observation highlights the issue of choosing the carrier wavenumber; some other choice, e.g. the median wavenumber, may lead to even better agreement.

4 Proof of Theorem 3.1

First of all observe that, by virtue of a simple gauge transform,

$$v^A(x_1, x_2, t) = e^{i(\kappa^A x_1 + \lambda^A x_2 + \tau^A t)} A(x_1, x_2, t), \quad v^B(x_1, x_2, t) = e^{i(\kappa^B x_1 + \lambda^B x_2 + \tau^B t)} B(x_1, x_2, t) \quad (20)$$

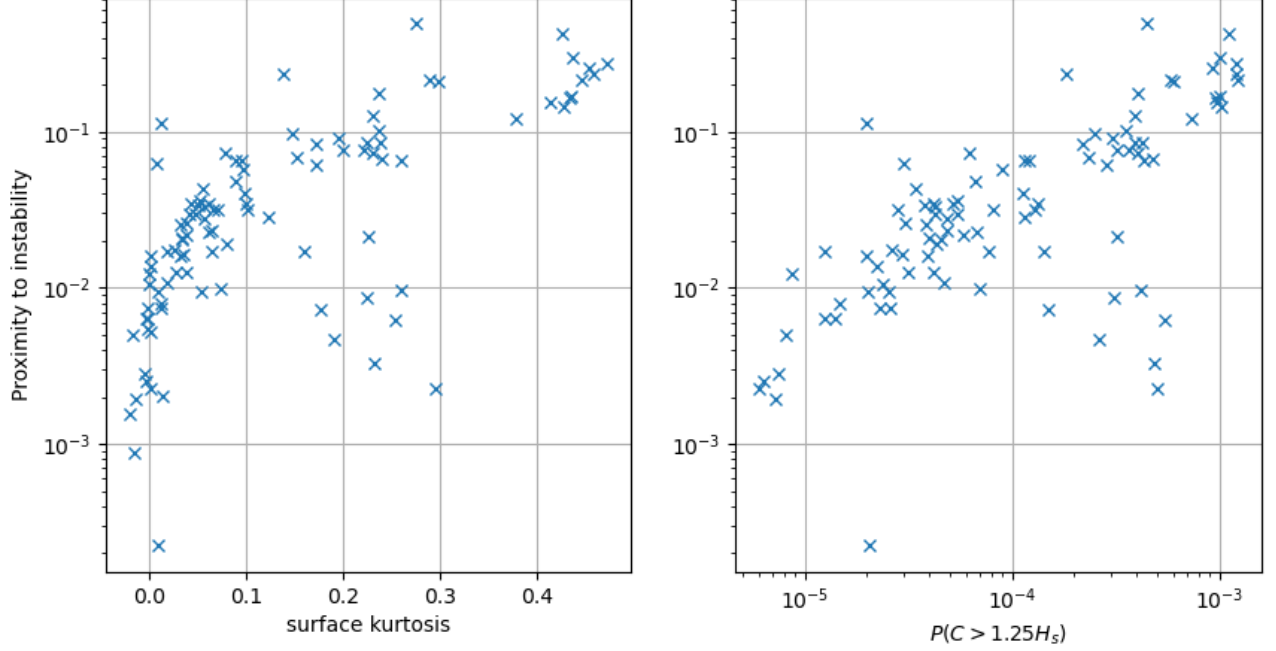


Figure 8: A Monte-Carlo simulation was performed with HOSM for each spectrum. This contains no narrowband assumptions or Gaussian closures, thus enabling us to put these assumptions in context; see Section 3.2.3 for more details. Two key metrics generated are the kurtosis and the probability of large waves. **Left:** lin-log scatterplot of kurtosis v. proximity to instability. Kurtosis can be interpreted as deviation from Gaussianity, which is associated with increased probability of nonlinear and / or extreme events. **Right:** log-log scatterplot of the probability of a wave-crest being larger than $1.25H_s$, an extreme event of probability of $O(10^{-6})$ in the linear / Gaussian setting. Both of these metrics correlate reasonably well with the new “proximity to instability” metric.

we can eliminate the terms with the first derivatives⁴; without loss of generality we will work with the simplified system

$$i \frac{d}{dt} A + \alpha_1 \partial_{x_1}^2 A + \beta_1 \partial_{x_2}^2 A + \gamma_1 \partial_{x_1} \partial_{x_2} A + (\xi_1 |A|^2 + \zeta_1 |B|^2) A = 0, \quad (21)$$

$$i \frac{d}{dt} B + \alpha_2 \partial_{x_1}^2 B + \beta_2 \partial_{x_2}^2 B + \gamma_2 \partial_{x_1} \partial_{x_2} B + (\xi_2 |B|^2 + \zeta_2 |A|^2) B = 0. \quad (22)$$

Special symmetric cases of this system which simplify the coefficients have been studied in [39, 47], but we can in fact derive an Alber system for the general case.

To proceed we will use some shorthand notations, namely

$$\mathbf{x} = (x_1, x_2), \quad \mathbf{y} = (y_1, y_2), \quad L_{\mathbf{x}}^j = \alpha_j \partial_{x_1}^2 + \beta_j \partial_{x_2}^2 + \gamma_j \partial_{x_1 x_2}, \quad j \in \{1, 2\}. \quad (23)$$

⁴By plugging (20) in eq. (13) we see that eliminating the linear terms containing A and ∇A leads to

$$\begin{aligned} \kappa^A 2\alpha_1 + \lambda^A \gamma_1 &= -C_1^A, \\ \kappa^A \gamma_1 + \lambda^A 2\beta_1 &= -C_2^A, \\ \tau &= -C_1^A \kappa^A - C_2^A \lambda^A - \alpha_1 (\kappa^A)^2 - \beta_1 (\lambda^A)^2 - \gamma_1 \kappa^A \lambda^A. \end{aligned}$$

The first two lines is a 2×2 system, and for the third, nonlinear equation we only need to substitute the obtained κ^A, λ^A values from above. The same steps lead to a symmetric expression for B .

Now equation (21) can be compactified as

$$i \frac{\partial A}{\partial t} + L_{\mathbf{x}}^1 A + (\xi_1 |A|^2 + \zeta_1 |B|^2) A = 0$$

and similarly for eq. (22) with $L_{\mathbf{x}}^2$.

At this point let us introduce the autocorrelation functions for A, B ;

$$R_A(\mathbf{x}, \mathbf{y}, t) = \mathbb{E}[A(\mathbf{x}, t) \overline{A}(\mathbf{y}, t)], \quad R_B(\mathbf{x}, \mathbf{y}, t) = \mathbb{E}[B(\mathbf{x}, t) \overline{B}(\mathbf{y}, t)]. \quad (24)$$

Observe that the relationship with the autocorrelations of the original v^A, v^B variables is

$$R_A(\mathbf{x}, \mathbf{y}, t) = e^{-i(\kappa^A(x_1 - y_1) + \lambda^A(x_2 - y_2))} \mathbb{E}[v^A(\mathbf{x}, t) \overline{v^A}(\mathbf{y}, t)] \quad (25)$$

and similarly for R_B .

By a straightforward computation we see that

$$\begin{aligned} \frac{d}{dt} R_A(\mathbf{x}, \mathbf{y}, t) &= \mathbb{E}[A(\mathbf{x}, t) \frac{d}{dt} \overline{A}(\mathbf{y}, t) + \overline{A}(\mathbf{y}, t) \frac{d}{dt} A(\mathbf{x}, t)] = \\ &= \mathbb{E}[A(\mathbf{x}, t) (-iL_{\mathbf{y}}^1 \overline{A}(\mathbf{y}, t) - i(\xi_1 |A(\mathbf{y}, t)|^2 + \zeta_1 |B(\mathbf{y}, t)|^2) \overline{A}(\mathbf{y}, t))] + \\ &\quad + \mathbb{E}[\overline{A}(\mathbf{y}, t) (iL_{\mathbf{x}}^1 A(\mathbf{x}, t) + i(\xi_1 |A(\mathbf{x}, t)|^2 + \zeta_1 |B(\mathbf{x}, t)|^2) A(\mathbf{x}, t))] = \\ &= i(L_{\mathbf{x}}^1 - L_{\mathbf{y}}^1) R_A(\mathbf{x}, \mathbf{y}, t) + \\ &\quad + i\xi_1 \mathbb{E}[|A(\mathbf{x}, t)|^2 A(\mathbf{x}, t) \overline{A}(\mathbf{y}, t)] - i\xi_1 \mathbb{E}[|A(\mathbf{y}, t)|^2 \overline{A}(\mathbf{y}, t) A(\mathbf{x}, t)] + \\ &\quad + i\zeta_1 \mathbb{E}[|B(\mathbf{x}, t)|^2 A(\mathbf{x}, t) \overline{A}(\mathbf{y}, t)] - i\zeta_1 \mathbb{E}[|B(\mathbf{y}, t)|^2 \overline{A}(\mathbf{y}, t) A(\mathbf{x}, t)]. \end{aligned}$$

The last two lines consist of fourth order stochastic moments, and it is these terms that will have to be approximated by some closure scheme. For the fourth order moments involving A only, we will use the same idea as in the standard Alber equation; namely we will use the fact that for Gaussian processes the relationship

$$\mathbb{E}[|A(\mathbf{x}, t)|^2 A(\mathbf{x}, t) \overline{A}(\mathbf{y}, t)] = 2R_A(\mathbf{x}, \mathbf{x}, t) R_A(\mathbf{x}, \mathbf{y}, t) \quad (26)$$

holds (cf. Theorem A.1). This now provides the Gaussian closure for all terms of the same form, since

$$\mathbb{E}[|A(\mathbf{y}, t)|^2 A(\mathbf{x}, t) \overline{A}(\mathbf{y}, t)] = 2R_A(\mathbf{y}, \mathbf{y}, t) R_A(\mathbf{x}, \mathbf{y}, t) \quad (27)$$

follows by the same argument. The new kinds of terms that come into play for the first time are the joint $A - B$ moments. In physical terms, A and B represent two different wavetrains meeting in the ocean, each having been generated and propagated independently from each other. It is thus a reasonable assumption that they are stochastically independent. In that case, the joint moments simplify to

$$\begin{aligned} \mathbb{E}[|B(\mathbf{x}, t)|^2 A(\mathbf{x}, t) \overline{A}(\mathbf{y}, t)] &= R_B(\mathbf{x}, \mathbf{x}, t) R_A(\mathbf{x}, \mathbf{y}, t), \\ \mathbb{E}[|B(\mathbf{y}, t)|^2 \overline{A}(\mathbf{y}, t) A(\mathbf{x}, t)] &= R_B(\mathbf{y}, \mathbf{y}, t) R_A(\mathbf{x}, \mathbf{y}, t). \end{aligned} \quad (28)$$

So, using these closures we finally end up with the following equation (whenever the independent variables are not shown explicitly, it is understood that $R_A := R_A(\mathbf{x}, \mathbf{y}, t)$):

$$\begin{aligned} i \frac{d}{dt} R_A + (L_{\mathbf{x}}^1 - L_{\mathbf{y}}^1) R_A + \\ + 2\xi_1 (R_A(\mathbf{x}, \mathbf{x}, t) - R_A(\mathbf{y}, \mathbf{y}, t)) R_A + 2\zeta_1 (R_B(\mathbf{x}, \mathbf{x}, t) - R_B(\mathbf{y}, \mathbf{y}, t)) R_A = 0. \end{aligned} \quad (29)$$

By the symmetry of equations (21), (22) one readily sees that, using the same kinds of closures,

$$\begin{aligned} i \frac{d}{dt} R_B + (L_{\mathbf{x}}^2 - L_{\mathbf{y}}^2) R_B + \\ + 2\xi_2 (R_B(\mathbf{x}, \mathbf{x}, t) - R_B(\mathbf{y}, \mathbf{y}, t)) R_B + 2\zeta_2 (R_A(\mathbf{x}, \mathbf{x}, t) - R_A(\mathbf{y}, \mathbf{y}, t)) R_B = 0. \end{aligned} \quad (30)$$

Now, we invoke the assumption of eq. (15), i.e.

$$R_A(\mathbf{x}, \mathbf{y}, t) = \Gamma^A(\mathbf{x} - \mathbf{y}) + \epsilon \rho(\mathbf{x}, \mathbf{y}, t), \quad R_B(\mathbf{x}, \mathbf{y}, t) = \Gamma^B(\mathbf{x} - \mathbf{y}) + \epsilon \sigma(\mathbf{x}, \mathbf{y}, t) \quad (31)$$

where now ρ, σ are the inhomogeneous components of the autocorrelation⁵ Observe that, under the condition (31), the system (29), (30) is equivalent to (like earlier, $\rho := \rho(\mathbf{x}, \mathbf{y}, t)$ and similarly for σ)

$$\begin{aligned} & i \frac{d}{dt} \rho + (L_{\mathbf{x}}^1 - L_{\mathbf{y}}^1) \rho + \\ & + 2\xi_1 (\rho(\mathbf{x}, \mathbf{x}, t) - \rho(\mathbf{y}, \mathbf{y}, t)) (\Gamma^A(\mathbf{x} - \mathbf{y}) + \epsilon \rho) + 2\zeta_1 (\sigma(\mathbf{x}, \mathbf{x}, t) - \sigma(\mathbf{y}, \mathbf{y}, t)) (\Gamma^A(\mathbf{x} - \mathbf{y}) + \epsilon \rho) = 0, \\ & i \frac{d}{dt} \sigma + (L_{\mathbf{x}}^2 - L_{\mathbf{y}}^2) \sigma + \\ & + 2\xi_2 (\sigma(\mathbf{x}, \mathbf{x}, t) - \sigma(\mathbf{y}, \mathbf{y}, t)) (\Gamma^B(\mathbf{x} - \mathbf{y}) + \epsilon \sigma) + 2\zeta_2 (\rho(\mathbf{x}, \mathbf{x}, t) - \rho(\mathbf{y}, \mathbf{y}, t)) (\Gamma^B(\mathbf{x} - \mathbf{y}) + \epsilon \sigma) = 0, \end{aligned} \quad (32)$$

and $\rho = \sigma = 0$ is a solution. Following the terminology of Wigner equations, the terms

$$n_A(\mathbf{y}, t) := \rho(\mathbf{y}, \mathbf{y}, t), \quad n_B(\mathbf{y}, t) := \sigma(\mathbf{y}, \mathbf{y}, t) \quad (33)$$

will be called **position densities**; they are real valued, and they control the RMS amplitude of the inhomogeneities, for each wavetrain, on the coordinates (\mathbf{y}, t) .

The question that we will focus on is whether $\rho = \sigma = 0$ is a linearly stable solution. To that end we will consider non-zero initial data $\rho(\mathbf{x}, \mathbf{y}, 0), \sigma(\mathbf{x}, \mathbf{y}, 0)$. We will also need to introduce the change of variables

$$\begin{aligned} \rho(\mathbf{x}, \mathbf{y}, t) &= \check{f}(\mathbf{p}, \mathbf{q}, t), \quad \sigma(\mathbf{x}, \mathbf{y}, t) = \check{g}(\mathbf{p}, \mathbf{q}, t) \\ \mathbf{p} &= \frac{\mathbf{x} + \mathbf{y}}{2}, \quad \mathbf{q} = \mathbf{x} - \mathbf{y} \end{aligned} \quad (34)$$

which leads to

$$\begin{aligned} \nabla_{\mathbf{x}} &= \frac{1}{2} \nabla_{\mathbf{p}} + \nabla_{\mathbf{q}}, \quad \nabla_{\mathbf{y}} = \frac{1}{2} \nabla_{\mathbf{p}} - \nabla_{\mathbf{q}}, \\ L_{\mathbf{x}}^j &= \alpha_j (\frac{1}{2} \partial_{p_1} + \partial_{q_1})^2 + \beta_j (\frac{1}{2} \partial_{p_2} + \partial_{q_2})^2 + \gamma_j (\frac{1}{2} \partial_{p_1} + \partial_{q_1}) (\frac{1}{2} \partial_{p_2} + \partial_{q_2}), \\ L_{\mathbf{y}}^j &= \alpha_j (\frac{1}{2} \partial_{p_1} - \partial_{q_1})^2 + \beta_j (\frac{1}{2} \partial_{p_2} - \partial_{q_2})^2 + \gamma_j (\frac{1}{2} \partial_{p_1} - \partial_{q_1}) (\frac{1}{2} \partial_{p_2} - \partial_{q_2}), \end{aligned} \quad (35)$$

$$\mathbf{x} = \mathbf{p} + \frac{\mathbf{q}}{2}, \quad \mathbf{y} = \mathbf{p} - \frac{\mathbf{q}}{2},$$

$$n_A(\mathbf{x}, t) = \rho(\mathbf{x}, \mathbf{x}, t) = \check{f}(\mathbf{x}, 0, t) = \check{f}(\mathbf{p} + \frac{\mathbf{q}}{2}, 0, t), \quad n_A(\mathbf{y}, t) = \rho(\mathbf{y}, \mathbf{y}, t) = \check{f}(\mathbf{p} - \frac{\mathbf{q}}{2}, 0, t),$$

and similarly for n_B . So finally we arrive at the following system in the \mathbf{p}, \mathbf{q} variables ($\check{f} := \check{f}(\mathbf{p}, \mathbf{q}, t)$, $\check{g} := \check{g}(\mathbf{p}, \mathbf{q}, t)$):

$$\begin{aligned} & i \frac{d}{dt} \check{f} + [2\alpha_1 \partial_{p_1} \partial_{q_1} + 2\beta_1 \partial_{p_2} \partial_{q_2} + \gamma_1 (\partial_{p_1} \partial_{q_2} + \partial_{p_2} \partial_{q_1})] \check{f} + \\ & + 2 \left[\xi_1 (\check{f}(\mathbf{p} + \frac{\mathbf{q}}{2}, 0, t) - \check{f}(\mathbf{p} - \frac{\mathbf{q}}{2}, 0, t)) + \zeta_1 (\check{g}(\mathbf{p} + \frac{\mathbf{q}}{2}, 0, t) - \check{g}(\mathbf{p} - \frac{\mathbf{q}}{2}, 0, t)) \right] (\Gamma^A(\mathbf{q}) + \epsilon \check{f}) = 0, \\ & i \frac{d}{dt} \check{g} + [2\alpha_2 \partial_{p_1} \partial_{q_1} + 2\beta_2 \partial_{p_2} \partial_{q_2} + \gamma_2 (\partial_{p_1} \partial_{q_2} + \partial_{p_2} \partial_{q_1})] \check{g} + \\ & + 2 \left[\xi_2 (\check{g}(\mathbf{p} + \frac{\mathbf{q}}{2}, 0, t) - \check{g}(\mathbf{p} - \frac{\mathbf{q}}{2}, 0, t)) + \zeta_2 (\check{f}(\mathbf{p} + \frac{\mathbf{q}}{2}, 0, t) - \check{f}(\mathbf{p} - \frac{\mathbf{q}}{2}, 0, t)) \right] (\Gamma^B(\mathbf{q}) + \epsilon \check{g}) = 0 \end{aligned} \quad (36)$$

Finally by and linearising (setting $\epsilon = 0$) and taking the Fourier transform in both variables,

$$f(\mathbf{P}, \mathbf{Q}, t) = \mathcal{F}_{\mathbf{p}, \mathbf{q} \rightarrow \mathbf{P}, \mathbf{Q}}[\check{f}(\mathbf{p}, \mathbf{q})], \quad g(\mathbf{P}, \mathbf{Q}, t) = \mathcal{F}_{\mathbf{p}, \mathbf{q} \rightarrow \mathbf{P}, \mathbf{Q}}[\check{g}(\mathbf{p}, \mathbf{q})], \quad (37)$$

⁵Recall that the conversion between second moments of A, B and v^A, v^B follows eq. (25).

we obtain

$$\begin{aligned}
i\frac{d}{dt}f - 4\pi^2 [2\alpha_1 P_1 Q_1 + 2\beta_1 P_2 Q_2 + \gamma_1 (P_1 Q_2 + P_2 Q_1)] f + \\
+ 2(\widehat{\Gamma^A}(\mathbf{Q} - \frac{\mathbf{P}}{2}) - \widehat{\Gamma^A}(\mathbf{Q} + \frac{\mathbf{P}}{2})) [\xi_1 \int f(\mathbf{P}, s, t) ds + \zeta_1 \int g(\mathbf{P}, s, t) ds] = 0, \\
i\frac{d}{dt}g - 4\pi^2 [2\alpha_2 P_1 Q_1 + 2\beta_2 P_2 Q_2 + \gamma_2 (P_1 Q_2 + P_2 Q_1)] g + \\
+ 2(\widehat{\Gamma^B}(\mathbf{Q} - \frac{\mathbf{P}}{2}) - \widehat{\Gamma^B}(\mathbf{Q} + \frac{\mathbf{P}}{2})) [\xi_2 \int g(\mathbf{P}, s, t) ds + \zeta_2 \int f(\mathbf{P}, s, t) ds] = 0
\end{aligned} \tag{38}$$

where of course $\widehat{\Gamma^A}(\mathbf{Q}) = \mathcal{F}_{\mathbf{q} \rightarrow \mathbf{Q}}[\Gamma^A(\mathbf{q})]$ and similarly for $\widehat{\Gamma^B}(\mathbf{Q})$. Observe moreover that

$$\int f(\mathbf{P}, s, t) ds = \mathcal{F}_{\mathbf{p} \rightarrow \mathbf{P}}^{-1}[n_A(\mathbf{p}, t)], \quad \int g(\mathbf{P}, s, t) ds = \mathcal{F}_{\mathbf{p} \rightarrow \mathbf{P}}^{-1}[n_B(\mathbf{p}, t)], \tag{39}$$

hence the notation

$$\tilde{n}_A(\mathbf{P}, t) := \int f(\mathbf{P}, s, t) ds, \quad \tilde{n}_B(\mathbf{P}, t) := \int g(\mathbf{P}, s, t) ds \tag{40}$$

is natural. Also in the interest of brevity let us introduce the bilinear forms

$$\langle \mathbf{P}, \mathbf{Q} \rangle_j := 4\pi^2 [2\alpha_j P_1 Q_1 + 2\beta_j P_2 Q_2 + \gamma_j (P_1 Q_2 + P_2 Q_1)], \quad j \in \{1, 2\}. \tag{41}$$

Now taking the Laplace transform in time

$$\begin{aligned}
\tilde{f}(\mathbf{P}, \mathbf{Q}, \omega) &= \mathcal{L}_{t \rightarrow \omega}[f(\mathbf{P}, \mathbf{Q}, t)], & \tilde{g}(\mathbf{P}, \mathbf{Q}, \omega) &= \mathcal{L}_{t \rightarrow \omega}[g(\mathbf{P}, \mathbf{Q}, t)], \\
\tilde{n}_A(\mathbf{P}, \omega) &= \mathcal{L}_{t \rightarrow \omega}[\tilde{n}_A(\mathbf{P}, t)], & \tilde{n}_B(\mathbf{P}, \omega) &= \mathcal{L}_{t \rightarrow \omega}[\tilde{n}_B(\mathbf{P}, t)]
\end{aligned} \tag{42}$$

we obtain the system

$$\begin{aligned}
i\omega \tilde{f} - \langle \mathbf{P}, \mathbf{Q} \rangle_1 \tilde{f} + 2(\widehat{\Gamma^A}(\mathbf{Q} - \frac{\mathbf{P}}{2}) - \widehat{\Gamma^A}(\mathbf{Q} + \frac{\mathbf{P}}{2})) [\xi_1 \tilde{n}_A(\mathbf{P}, \omega) + \zeta_1 \tilde{n}_B(\mathbf{P}, \omega)] &= f(\mathbf{P}, \mathbf{Q}, 0), \\
i\omega \tilde{g} - \langle \mathbf{P}, \mathbf{Q} \rangle_2 \tilde{g} + 2(\widehat{\Gamma^B}(\mathbf{Q} - \frac{\mathbf{P}}{2}) - \widehat{\Gamma^B}(\mathbf{Q} + \frac{\mathbf{P}}{2})) [\xi_2 \tilde{n}_B(\mathbf{P}, \omega) + \zeta_2 \tilde{n}_A(\mathbf{P}, \omega)] &= g(\mathbf{P}, \mathbf{Q}, 0).
\end{aligned} \tag{43}$$

By dividing with the free-space part we obtain

$$\begin{aligned}
\tilde{f} + 2 \frac{\widehat{\Gamma^A}(\mathbf{Q} - \frac{\mathbf{P}}{2}) - \widehat{\Gamma^A}(\mathbf{Q} + \frac{\mathbf{P}}{2})}{i\omega - \langle \mathbf{P}, \mathbf{Q} \rangle_1} [\xi_1 \tilde{n}_A + \zeta_1 \tilde{n}_B] &= \frac{f(\mathbf{P}, \mathbf{Q}, 0)}{i\omega - \langle \mathbf{P}, \mathbf{Q} \rangle_1}, \\
\tilde{g} + 2 \frac{\widehat{\Gamma^B}(\mathbf{Q} - \frac{\mathbf{P}}{2}) - \widehat{\Gamma^B}(\mathbf{Q} + \frac{\mathbf{P}}{2})}{i\omega - 4\pi^2 \langle \mathbf{P}, \mathbf{Q} \rangle_2} [\xi_2 \tilde{n}_B + \zeta_2 \tilde{n}_A] &= \frac{g(\mathbf{P}, \mathbf{Q}, 0)}{i\omega - \langle \mathbf{P}, \mathbf{Q} \rangle_2}.
\end{aligned} \tag{44}$$

The two key observations here are the following:

- the rhs of both equations correspond to the linear free-space solutions (and thus can be treated as known and well-behaved functions), moreover
- we can now integrate both equations in the \mathbf{Q} variables and **obtain a closed system for the position densities \tilde{n}_A, \tilde{n}_B ; achieving this is in fact the motivation for all the transforms and changes of variables.**

$$\begin{aligned}
\tilde{n}_A + [\xi_1 \tilde{n}_A + \zeta_1 \tilde{n}_B] 2 \int_{\mathbf{Q}} \frac{\widehat{\Gamma^A}(\mathbf{Q} - \frac{\mathbf{P}}{2}) - \widehat{\Gamma^A}(\mathbf{Q} + \frac{\mathbf{P}}{2})}{i\omega - \langle \mathbf{P}, \mathbf{Q} \rangle_1} d\mathbf{Q} &= \int_{\mathbf{Q}} \frac{f(\mathbf{P}, \mathbf{Q}, 0)}{i\omega - \langle \mathbf{P}, \mathbf{Q} \rangle_1} d\mathbf{Q}, \\
\tilde{n}_B + [\xi_2 \tilde{n}_B + \zeta_2 \tilde{n}_A] 2 \int_{\mathbf{Q}} \frac{\widehat{\Gamma^B}(\mathbf{Q} - \frac{\mathbf{P}}{2}) - \widehat{\Gamma^B}(\mathbf{Q} + \frac{\mathbf{P}}{2})}{i\omega - \langle \mathbf{P}, \mathbf{Q} \rangle_2} d\mathbf{Q} &= \int_{\mathbf{Q}} \frac{g(\mathbf{P}, \mathbf{Q}, 0)}{i\omega - \langle \mathbf{P}, \mathbf{Q} \rangle_2} d\mathbf{Q}.
\end{aligned} \tag{45}$$

We can summarize the result by denoting

$$\begin{aligned}\tilde{n}_A^0(\mathbf{P}, \omega) &:= \int_{\mathbf{Q}} \frac{f(\mathbf{P}, \mathbf{Q}, 0)}{i\omega - \langle \mathbf{P}, \mathbf{Q} \rangle_1} d\mathbf{Q}, & \tilde{n}_B^0(\mathbf{P}, \omega) &:= \int_{\mathbf{Q}} \frac{g(\mathbf{P}, \mathbf{Q}, 0)}{i\omega - \langle \mathbf{P}, \mathbf{Q} \rangle_2} d\mathbf{Q}, \\ h^A(\mathbf{P}, \omega) &:= 2 \int_{\mathbf{Q}} \frac{\widehat{\Gamma}^A(\mathbf{Q} + \frac{\mathbf{P}}{2}) - \widehat{\Gamma}^A(\mathbf{Q} - \frac{\mathbf{P}}{2})}{i\omega - \langle \mathbf{P}, \mathbf{Q} \rangle_1} d\mathbf{Q}, & h^B(\mathbf{P}, \omega) &:= 2 \int_{\mathbf{Q}} \frac{\widehat{\Gamma}^B(\mathbf{Q} + \frac{\mathbf{P}}{2}) - \widehat{\Gamma}^B(\mathbf{Q} - \frac{\mathbf{P}}{2})}{i\omega - \langle \mathbf{P}, \mathbf{Q} \rangle_2} d\mathbf{Q}\end{aligned}\quad (46)$$

so that system (45) becomes

$$\left\{ \begin{array}{l} (1 - \xi_1 h^A) \tilde{n}_A - \zeta_1 h^A \tilde{n}_B = \tilde{n}_A^0, \\ -\zeta_2 h^B \tilde{n}_A + (1 - \xi_2 h^B) \tilde{n}_B = \tilde{n}_B^0 \end{array} \right\} \quad (47)$$

leading to

$$\begin{aligned}\tilde{n}_A &= \frac{1 - \xi_2 h^B}{(1 - \xi_1 h^A)(1 - \xi_2 h^B) - \zeta_1 \zeta_2 h^A h^B} \tilde{n}_A^0 + \frac{\zeta_1 h^A}{(1 - \xi_1 h^A)(1 - \xi_2 h^B) - \zeta_1 \zeta_2 h^A h^B} \tilde{n}_B^0, \\ \tilde{n}_B &= \frac{-\zeta_2 h^B}{(1 - \xi_1 h^A)(1 - \xi_2 h^B) - \zeta_1 \zeta_2 h^A h^B} \tilde{n}_A^0 - \frac{1 - \xi_1 h^A}{(1 - \xi_1 h^A)(1 - \xi_2 h^B) - \zeta_1 \zeta_2 h^A h^B} \tilde{n}_B^0\end{aligned}\quad (48)$$

as long as the determinant (itself a function of \mathbf{P}, ω) is nonzero,

$$(1 - \xi_1 h^A(\mathbf{P}, \omega))(1 - \xi_2 h^B(\mathbf{P}, \omega)) - \zeta_1 \zeta_2 h^A(\mathbf{P}, \omega) h^B(\mathbf{P}, \omega) \neq 0.$$

So the problem is altogether linearly stable if eqs. (17), (18) hold.

If both conditions (17), (18) hold, then

$$\tilde{n}_A(\mathbf{P}, t) = \mathcal{L}^{-1}[\tilde{n}_A(\mathbf{P}, \omega)], \quad \tilde{n}_B(\mathbf{P}, t) = \mathcal{L}^{-1}[\tilde{n}_B(\mathbf{P}, \omega)] \quad (49)$$

inherit an L^2 -type decay in time, and one expects that Landau damping estimates similar to what was done in the scalar case in [7] are possible. Even without the rigorous estimates one readily sees that there is no exponential growth possible, i.e. no modulation instability.

5 Conclusions

- All the non-parametric spectra in the dataset we examined are found to be stable, but less than an order of magnitude away from instability.
- The spectral shape matters, especially for bimodal spectra or other shapes that are not very strongly unimodal; see Figure 3.
- BFI and steepness both do a good job of predicting the proximity to instability for unimodal spectra, but less so for bimodal spectra. The maximum value of the rescaled spectrum does a very good job of predicting proximity to instability; see Figure 7.
- A phase-resolved Monte Carlo simulation using HOSM shows good correlation of proximity to instability with probability of extreme waves and non-Gaussianity. In particular, this justifies to an extent the approximations involved in the derivation of the Alber equation. See Figure 8.
- A generalized Alber equation for crossing seas is possible, and it generates a 2D version of the instability condition. Thus a 2D version of the analysis behind Definition 2.1 will be needed to resolve it.
- Choosing the carrier wavenumber k_0 , or each of the two carrier wavenumbers $\mathbf{k}_A, \mathbf{k}_B$ in the crossing seas scenario, may introduce some ambiguity in the results. This point is further reinforced by the comparison with phase-resolved Monte Carlo simulations. A clear way around this limitation would be working with a broadband moment equation. The CSY equation is in many ways analogous to the Alber equation, but it is broadband (i.e. no need to choose carrier wavenumbers). It was further recently indicated to have an instability condition analogous to Alber's instability condition [4]. Developing a constructive technique to resolve that instability condition is a natural next step.

Acknowledgement: We thank the Norwegian Meteorological Institute for providing the wave model spectra used in this study.

References

- [1] T. ALAZARD, N. BURQ, AND C. ZUILY, *On the Cauchy problem for gravity water waves*, *Inventiones Mathematicae*, 198 (2014), pp. 71–163.
- [2] I. E. ALBER, *The Effects of Randomness on the Stability of Two-Dimensional Surface Wavetrains*, *Proceedings of the Royal Society A: Mathematical, Physical and Engineering Sciences*, 363 (1978), pp. 525–546.
- [3] D. ANDRADE AND M. STIASSNIE, *Bound-waves due to sea and swell trigger the generation of freak-waves*, *Journal of Ocean Engineering and Marine Energy*, 6 (2020), pp. 399–414.
- [4] ———, *New solutions of the C.S.Y. equation reveal increases in freak wave occurrence*, *Wave Motion*, 97 (2020), p. 102581.
- [5] A. ANKIEWICZ, D. J. KEDZIORA, AND N. AKHMEDIEV, *Rogue wave triplets*, *Physics Letters, Section A: General, Atomic and Solid State Physics*, 375 (2011), pp. 2782–2785.
- [6] A. ARMAROLI, D. EELTINK, AND M. BRUNETTI, *Nonlinear stage of Benjamin-Feir instability in forced / damped deep-water waves*, *Physics of Fluids*, 30 (2018), p. 017102.
- [7] A. G. ATHANASSOULIS, G. A. ATHANASSOULIS, M. PTASHNYK, AND T. SAPSIS, *Strong solutions for the Alber equation and stability of unidirectional wave spectra*, *Kinetic & Related Models*, 13 (2020), pp. 703–737.
- [8] A. G. ATHANASSOULIS, G. A. ATHANASSOULIS, AND T. SAPSIS, *Localized instabilities of the Wigner equation as a model for the emergence of Rogue Waves*, *Journal of Ocean Engineering and Marine Energy*, 3 (2017), pp. 353–372.
- [9] G. A. ATHANASSOULIS AND K. A. BELIBASSAKIS, *A consistent coupled-mode theory for the propagation of small-amplitude water waves over variable bathymetry regions*, 389 (1999), pp. 275–301.
- [10] D. J. BENNEY AND A. C. NEWELL, *The propagation of nonlinear wave envelopes*, *Studies in Applied Mathematics*, 46 (1967), pp. 133–139.
- [11] E. M. BITNER-GREGERSEN, O. GRAMSTAD, A. K. MAGNUSSON, AND P. C. SAMES, *Occurrence Frequency of a Triple Rogue Wave Group in the Ocean*, aug 2020.
- [12] J. C. BORGE, G. RODRÍQUEZ RODRÍGUEZ, K. HESSNER, AND P. I. GONZÁLEZ, *Inversion of marine radar images for surface wave analysis*, *Journal of Atmospheric and Oceanic Technology*, 21 (2004), pp. 1291–1300.
- [13] M. BRUNETTI AND J. KASPARIAN, *Modulational instability in wind-forced waves*, *Physics Letters, Section A: General, Atomic and Solid State Physics*, 378 (2014), pp. 3626–3630.
- [14] M. BRUNETTI, N. MARCHIANDO, N. BERTI, AND J. KASPARIAN, *Nonlinear fast growth of water waves under wind forcing*, *Physics Letters, Section A: General, Atomic and Solid State Physics*, 378 (2014), pp. 1025–1030.
- [15] O. BÜHLER, J. SHATAH, S. WALSH, AND C. ZENG, *On the Wind Generation of Water Waves*, *Archive for Rational Mechanics and Analysis*, 222 (2016), pp. 827–878.

- [16] C. M. CHIANG, M. STIASSNIE, AND D. K.-P. YUE, *Theory and Applications of Ocean Surface Waves*, vol. 23 of Advanced Series on Ocean Engineering, World Scientific, jul 2005.
- [17] G. F. CLAUSS, *Dramas of the sea: Episodic waves and their impact on offshore structures*, Applied Ocean Research, 24 (2002), pp. 147–161.
- [18] D. R. CRAWFORD, P. G. SAFFMAN, AND H. C. YUEN, *Evolution of a random inhomogeneous field of nonlinear deep-water gravity waves*, Wave Motion, 2 (1980), pp. 1–16.
- [19] G. DEMATTEIS, T. GRAFKE, AND E. VANDEN-EIJNDEN, *Rogue Waves and Large Deviations in Deep Sea*, Proceedings of the National Academy of Sciences, (2018), p. 201710670.
- [20] D. G. DOMMERMUTH AND D. K. P. YUE, *A high-order spectral method for the study of nonlinear gravity waves*, Journal of Fluid Mechanics, 184 (1987), pp. 267–288.
- [21] M. GOUIN, G. DUCROZET, AND P. FERRANT, *Development and validation of a non-linear spectral model for water waves over variable depth*, European Journal of Mechanics-B/Fluids, 57 (2016), pp. 115–128.
- [22] O. GRAMSTAD, *Modulational Instability in JONSWAP Sea States Using the Alber Equation*, in ASME 2017 36th International Conference on Ocean, Offshore and Arctic Engineering, 2017.
- [23] O. GRAMSTAD, E. BITNER-GREGERSEN, K. TRULSEN, AND J. C. NIETO BORGE, *Modulational Instability and Rogue Waves in Crossing Sea States*, Journal of Physical Oceanography, 48 (2018), pp. 1317–1331.
- [24] D. GREENSLADE, M. HEMER, A. BABANIN, R. LOWE, I. TURNER, H. POWER, I. YOUNG, D. IERODIACONOU, G. HIBBERT, G. WILLIAMS, S. AIJAZ, J. ALBUQUERQUE, S. ALLEN, M. BANNER, P. BRANSON, S. BUCHAN, A. BURTON, J. BYE, N. CARTWRIGHT, A. CHABCHOUB, F. COLBERG, S. CONTARDO, F. DUFOIS, C. EARL-SPURR, D. FARR, I. GOODWIN, J. GUNSON, J. HANSEN, D. HANSLOW, M. HARLEY, Y. HETZEL, R. HOEKE, N. JONES, M. KINSELA, Q. LIU, O. MAKARYNSKY, H. MARCOLLO, S. MAZAHARI, J. MCCONOCHE, G. MILLAR, T. MOLT-MANN, N. MOODIE, J. MORIM, R. MORISON, J. ORSZAGHOVA, C. PATTIARATCHI, A. POMEROY, R. PROCTOR, D. PROVIS, R. REEF, D. RIJNSDORP, M. RUTHERFORD, E. SCHULZ, J. SHAYER, K. SPLINTER, C. STEINBERG, D. STRAUSS, G. STUART, G. SYMONDS, K. TARBATH, D. TAYLOR, J. TAYLOR, D. THOTAGAMUWAGE, A. TOFFOLI, A. VALIZADEH, J. VAN HAZEL, G. V. DA SILVA, M. WANDRES, C. WHITTAKER, D. WILLIAMS, G. WINTER, J. XU, A. ZHONG, AND S. ZIEGER, *15 Priorities for Wind-Waves Research: An Australian Perspective*, Bulletin of the American Meteorological Society, 101, pp. E446 – E461.
- [25] J. L. HAMMACK, D. M. HENDERSON, AND H. SEGUR, *Progressive waves with persistent two-dimensional surface patterns in deep water*, Journal of Fluid Mechanics, 532 (2005), pp. 1–52.
- [26] K. HASSELMANN, *On the non-linear energy transfer in a gravity-wave spectrum Part 1. General theory*, Journal of Fluid Mechanics, 12 (1962), pp. 481–500.
- [27] P. A. E. M. JANSSEN, *The interaction of ocean waves and wind*, Cambridge University Press, Cambridge, 2004.
- [28] P. A. E. M. JANSSEN AND J.-R. BIDLOT, *On the extension of the freak wave warning system and its verification*, tech. rep., European Centre for Medium-Range Weather Forecasts (ECMWF), 2009.
- [29] G. J. KOMEN, L. CAVALERI, M. DONELAN, K. HASSELMANN, S. HASSELMANN, AND P. A. E. M. JANSSEN, *Dynamics and Modelling of Ocean Waves*, Cambridge University Press, 1994.

- [30] J. LABEYRIE, *Stationary and transient states of random seas*, Marine Structures, 3 (1990), pp. 43–58.
- [31] D. LANNES, *Well-posedness of the water-waves equations*, Journal of the American Mathematical Society, 18 (2005), pp. 605–654.
- [32] J. C. LUKE, *A variational principle for a fluid with a free surface*, Journal of Fluid Mechanics, 27 (1967), pp. 395–397.
- [33] A. K. MAGNUSSON, K. TRULSEN, O. J. AARNES, E. M. BITNER-GREGERSEN, AND M. P. MALILA, *“Three Sisters” Measured As a Triple Rogue Wave Group*, jun 2019.
- [34] K. MILLER, *Moments of complex Gaussian processes*, Proceedings of the IEEE, 56 (1968), pp. 83–84.
- [35] P. MÜLLER, C. GARRETT, AND A. OSBORNE, *Rogue waves-The Fourteenth ‘Aha Huliko’a Hawaiian Winter Workshop*, Oceanography, 18 (2005), pp. 66–75.
- [36] I. NIKOLKINA AND I. DIDENKULOVA, *Rogue waves in 2006-2010*, Natural Hazards and Earth System Sciences, 11 (2011), pp. 2913–2924.
- [37] M. K. OCHI, *Ocean Waves : the Stochastic Approach*, Cambridge University Press, 1998.
- [38] M. ONORATO, A. OSBORNE, R. FEDELE, AND M. SERIO, *Landau damping and coherent structures in narrow-banded 1 + 1 deep water gravity waves*, Physical Review E, 67 (2003), p. 046305.
- [39] M. ONORATO, A. R. OSBORNE, AND M. SERIO, *Modulational Instability in Crossing Sea States: A Possible Mechanism for the Formation of Freak Waves*, Physical Review Letters, 96 (2006), p. 014503.
- [40] M. ONORATO, D. PROMENT, AND A. TOFFOLI, *Freak waves in crossing seas*, European Physical Journal: Special Topics, 185 (2010), pp. 45–55.
- [41] M. ONORATO, S. RESIDORI, U. BORTOLOZZO, A. MONTINA, AND F. T. ARECCHI, *Rogue waves and their generating mechanisms in different physical contexts*, 2013.
- [42] M. ONORATO, T. WASEDA, A. TOFFOLI, L. CAVALERI, O. GRAMSTAD, P. A. JANSSEN, T. KINOSHITA, J. MONBALIU, N. MORI, A. R. OSBORNE, M. SERIO, C. T. STANSBERG, H. TAMURA, AND K. TRULSEN, *Statistical properties of directional ocean waves: The role of the modulational instability in the formation of extreme events*, Physical Review Letters, 102 (2009).
- [43] O. PENROSE, *Electrostatic Instabilities of a Uniform Non-Maxwellian Plasma*, Physics of Fluids, 3 (1960), pp. 258–265.
- [44] I. S. REED, *On a Moment Theorem for Complex Gaussian Processes*, IRE Transactions on Information Theory, 8 (1962), pp. 194–195.
- [45] M. REISTAD, Ø. BREIVIK, H. HAAKENSTAD, O. J. AARNES, B. R. FUREVIK, AND J.-R. BIDLOT, *A high-resolution hindcast of wind and waves for the North Sea, the Norwegian Sea, and the Barents Sea*, J. Geophys. Res. Oceans, 116 (2011).
- [46] A. RIBAL, A. V. BABANIN, I. YOUNG, A. TOFFOLI, AND M. STIASSNIE, *Recurrent solutions of the Alber equation initialized by Joint North Sea Wave Project spectra*, Journal of Fluid Mechanics, 719 (2013), pp. 314–344.
- [47] J. N. STEER, M. L. MCALLISTER, A. G. L. BORTHWICK, AND T. S. V. D. BREMER, *Experimental Observation of Modulational Instability in Crossing Surface Gravity Wavetrains*, Fluids, 4 (2019), pp. 1–15.

- [48] R. STUHLMEIER, T. VRECICA, AND Y. TOLEDO, *Nonlinear Wave Interaction in Coastal and Open Seas: Deterministic and Stochastic Theory*, in Nonlinear Water Waves, Springer, 2019, pp. 151–181.
- [49] A. TOFFOLI, O. GRAMSTAD, K. TRULSEN, J. MONBALIU, E. BITNER-GREGERSEN, AND M. ONORATO, *Evolution of weakly nonlinear random directional waves: Laboratory experiments and numerical simulations*, Journal of Fluid Mechanics, 664 (2010), pp. 313–336.
- [50] J. TOURNADRE, *Time and space scales of significant wave heights*, J. Geophys. Res., 98 (1993), pp. 4727–4738.
- [51] K. TRULSEN AND K. B. DYSTHE, *A modified nonlinear Schrödinger equation for broader bandwidth gravity waves on deep water*, Wave Motion, 24 (1996), pp. 281–289.
- [52] B. J. WEST, K. A. BRUECKNER, R. S. JANDA, D. M. MILDER, AND R. L. MILTON, *A new numerical method for surface hydrodynamics*, Journal of Geophysical Research: Oceans, 92 (1987), pp. 11803–11824.
- [53] V. E. ZAKHAROV, *Stability of periodic waves of finite amplitude on the surface of a deep fluid*, Journal of Applied Mechanics and Technical Physics, 9 (1968), pp. 190–194.
- [54] V. E. ZAKHAROV AND L. A. OSTROVSKY, *Modulation instability: The beginning*, Physica D: Nonlinear Phenomena, 238 (2009), pp. 540–548.

A Background

Theorem A.1 (A complex Isselris theorem). *Following [44]; see also [34]. Let $z(x)$ be a Gaussian, zero-mean, stationary process with the additional property that*

$$E[u(x)u(x')] = 0 \quad \forall x, x' \in \mathbb{R}. \quad (50)$$

Then

$$E[\overline{z(x_1)z(x_2)}z(x_3)z(x_4)] = E[\overline{z(x_1)z(x_3)}]E[\overline{z(x_2)z(x_4)}] + E[\overline{z(x_2)z(x_3)}]E[\overline{z(x_1)z(x_4)}].$$

Remark: This result directly implies the closure relation

$$E[\overline{u(\alpha, t)u(\beta, t)}u(\alpha, t)u(\alpha, t)] = 2E[\overline{u(\alpha, t)u(\alpha, t)}]E[\overline{u(\beta, t)u(\alpha, t)}], \quad (51)$$

which is exactly equation (3). Moreover, the condition (50) is equivalent to *circular symmetry*, i.e. to the condition that

$$\{e^{i\theta}u(x)\}_{\theta \in [0, 2\pi)} \text{ are identically distributed for all } \theta \in [0, 2\pi) \quad (52)$$

which is natural for ocean waves.